3257

3-D Numerical Simulation of Turbulent Air Flow in and around Buildings Based on the k-ε Model with Generalized Curvilinear Coordinates

S. Murakami, Dr. Eng. **S. Kato, Dr. Eng.** **Y. Ishida**

ABSTRACT

The air distribution in and around a building with a complicated configuration is well simulated by the finite difference method based on generalized curvilinear coordinates. This paper follows preceding studies which were based on ordinary Cartesian coordinates (Murakami et al. 1987, 1988).

Numerical simulations of room airflow by the present method using the k-ε model based on curvilinear coordinates are conducted. Its validity and feasibility for application to engineering problems are confirmed by comparing simulation results with the experimental results.

INTRODUCTION

In the numerical analysis of a flow field using the finite difference method (FDM) or another discretization method, fitting the grid discretization to complicated boundary configurations is one of the most important problems. While discretization based on Cartesian coordinates, which are composed solely of rectangular grids, can be applied only to simple configurations, it can be performed very easily and freely when generalized curvilinear coordinates are applied. The generalized curvilinear coordinates allow the grid system to fit the shape of any physical region of interest very smoothly. Cartesian coordinates are a particular case of the generalized curvilinear coordinates.

The authors have already submitted to *ASHRAE Transactions* three papers which evaluate the numerical simulation of room airflow based on the usual Cartesian coordinates (Murakami et al. 1987, 1988; Kato et al. 1988). This paper is the fourth in this series and is concerned with the method of numerical simulation of air distribution in and around a building with complicated boundary configurations.

Numerical analysis of flow fields using generalized curvilinear coordinates is popular in aeronautical engineering (e.g., Rizk 1985; Thompson et al. 1985). However, there are few studies using generalized curvilinear coordinates in which the transport equations for statistical turbulence properties, for example, the k-ε model equations (Yeung and Kot 1985; Murakami et al. 1988), are included. This may be partly because the method for numerical analysis, which includes the turbulence statistical variables as unknowns, meets with some difficulty in determining the boundary conditions in the case of generalized curvilinear coordinates. Now a computer program based on the curvilinear coordinate system has been developed which deals with those difficulties.

In this paper, three-dimensional turbulence flows are analyzed with the k-ε model equations based on generalized curvilinear coordinates. Three examples of numerical simulations are presented.

First, to confirm the applicability of the present method, numerical simulations of the room airflow are conducted. The room space is cubic. The simulations are then compared with results obtained by the existing numerical method, which is based on Cartesian coordinates using a staggered grid system, as well as with the experimental results. Good agreement is shown in these comparisons.

Second, a simulation of airflow in a gymnasium, which has a complicated globular boundary configuration, is performed. The results clearly demonstrate the practicability of the present method based on the curvilinear coordinate system. It gives reasonable airflow distributions for a three-dimensional non-rectangular space.

Finally, airflow distributions around a two-dimensional building model are presented. A separation at the upwind corner of the model and a wake behind it are reproduced with reasonable accuracy. This example shows the possibility of three-dimensional simulations of external airflow distributions around arbitrarily shaped buildings.

In the appendices the authors illustrate the procedures for transforming the k-ε model equations from Cartesian coordinates to a general curvilinear coordinate system, the method of discretization, the method of imposing boundary conditions, and the time marching pro-

S. Murakami is Professor and **S. Kato** is Associate Professor, Institute of Industrial Science, University of Tokyo, Japan; **Y. Ishida** Joint Researcher, Institute of Industrial Science, University of Tokyo, and Research Engineer, Information Processing Center, Kajima , Japan.

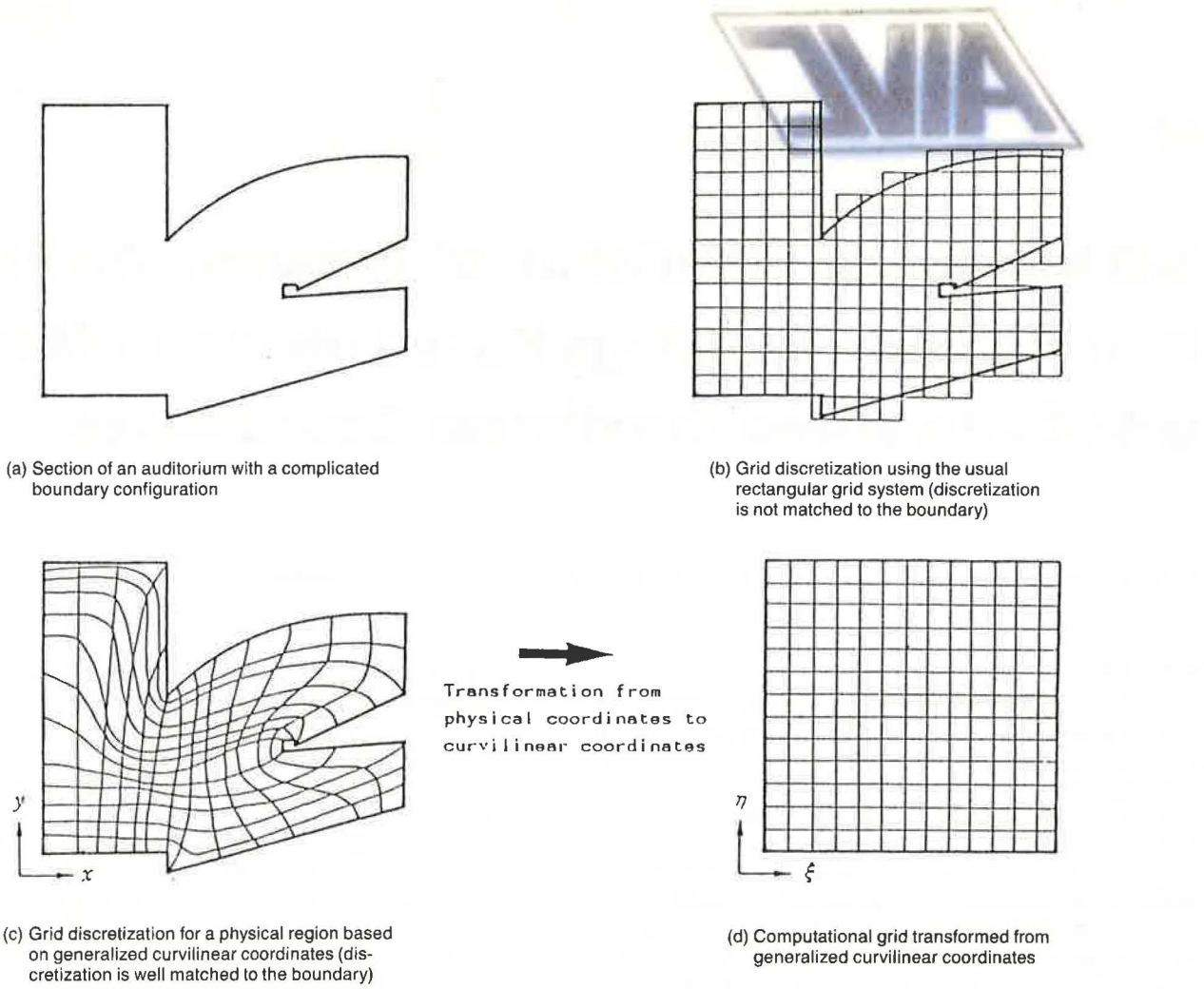

(a) Section of an auditorium with a complicated boundary configuration

(b) Grid discretization using the usual rectangular grid system (discretization is not matched to the boundary)

(c) Grid discretization for a physical region based on generalized curvilinear coordinates (discretization is well matched to the boundary)

(d) Computational grid transformed from generalized curvilinear coordinates

Figure 1 *Utilization of generalized curvilinear coordinates for airflow analysis of a room with a complicated boundary configuration*

cedure used to obtain steady-state solutions. The new conservative expression of the partial derivatives, highly recommended in order to ensure accuracy of the numerical integrations, is achieved here. Discretization of dependent variables (u, v, w, p, k, and ϵ) using the control volume method and formulations of the boundary conditions (i.e., wall law or wall function) are proposed. The Poisson equation for pressure is formulated, where the second-order derivatives of the pressure are integrated conservatively over each control volume. The pressure at the boundary is solved as an unknown. Errors related to the continuity condition of the control volumes adjacent to the boundary are thus markedly reduced.

We impose the effect of the wall boundary on the governing equations using the wall law or the wall function. Thus, we reset the imaginary computational boundary just inside of the physical region, leaving a small distance between the computational region and the physical region. In this way, we can formulate the imposition of boundary conditions on three-dimensional curved surfaces by means of a simple expression.

A fully implicit scheme is applied to the governing equations for the time marching procedure to obtain the steady-state solution. The utilization of a fully implicit scheme requires that the following equations be relaxed simultaneously: momentum equations; the Poisson equation for pressure; the transport equations of the turbulence kinetic energy, k; and the turbulence dissipation rate, ϵ. We solve these equations simultaneously using the overrelaxation method, which is very simple and converges well.

GENERALIZED CURVILINEAR COORDINATE SYSTEM

Architecture usually has a very complicated configuration, regardless of whether it is an indoor or an outdoor space. The usual rectangular grid discretization method is not good in matching the grid system to a complicated configuration, as shown in Figures 1a and 1b. A generalized curvilinear coordinate system makes it possible to form a very smooth curve-fitting discretization, as shown in Figure 1c. The complicated physical region of Figure 1c is transformed into a rectangular computational grid region by means of curvilinear coordinates, as shown in Figure 1d. Numerical computation is conducted on this simple rectangular grid system.

Three-dimensional governing equations of the k-ϵ model with generalized curvilinear coordinates are proposed with the conservative expressions of each transport term. The computational program is developed by this method. The transformation procedures and the method of numerical analysis are described in detail in the appen-

TABLE 1
Governing Equations of the k-ϵ Model with Generalized Curvilinear Coordinates

CONTINUITY EQUATION

$$u_x+v_y+w_z$$
$$=[\{J(\xi_x u+\xi_y v+\xi_z w)\}_\xi+\{J(\eta_x u+\eta_y v+\eta_z w)\}_\eta+\{J(\zeta_x u+\zeta_y v+\zeta_z w)\}_\zeta]/J$$
$$=\{(JU)_\xi+(JV)_\eta+(JW)_\zeta\}/J=0 \tag{1.1}$$

Transformation Relations between the Contravariant Vector and the Usual Vector of Velocity

$$U=\xi_x u+\xi_y v+\xi_z w,\quad V=\eta_x u+\eta_y v+\eta_z w,\quad W=\zeta_x u+\zeta_y v+\zeta_z w \tag{1.2}$$
$$u=x_\xi U+x_\eta V+x_\zeta W,\ v=y_\xi U+y_\eta V+y_\zeta W,\ w=z_\xi U+z_\eta V+z_\zeta W \tag{1.3}$$

MOMENTUM EQUATIONS

$$u_t+HX=-p_x+FX \tag{1.4}$$
$$v_t+HY=-p_y+FY \tag{1.5}$$
$$w_t+HZ=-p_z+FZ \tag{1.6}$$

Convection Terms of the Momentum Equations

$$HX=(uu)_x+(uv)_y+(uw)_z$$
$$=\{(JUu)_\xi+(JVu)_\eta+(JWu)_\zeta\}/J \tag{1.7}$$
$$HY=(uv)_x+(vv)_y+(vw)_z$$
$$=\{(JUv)_\xi+(JVv)_\eta+(JWv)_\zeta\}/J \tag{1.8}$$
$$HZ=(uw)_x+(vw)_y+(ww)_z$$
$$=\{(JUw)_\xi+(JVw)_\eta+(JWw)_\zeta\}/J \tag{1.9}$$

Pressure Gradients of the Momentum Equations

$$p_x=\{(J\xi_x p)_\xi+(J\eta_x p)_\eta+(J\zeta_x p)_\zeta\}/J \tag{1.10}$$

TABLE 1 (*Continued*)
Governing Equations of the k-ε Model with Generalized Curvilinear Coordinates

$$p_y = \{(J\xi_y p)_\xi + (J\eta_y p)_\eta + (J\zeta_y p)_\zeta\}/J \tag{1.11}$$

$$p_z = \{(J\xi_z p)_\xi + (J\eta_z p)_\eta + (J\zeta_z p)_\zeta\}/J \tag{1.12}$$

Diffusion Terms of the Momentum Equations

$$\begin{aligned} FX &= \{\nu_t(2u_x)\}_x + \{\nu_t(u_y+v_x)\}_y + \{\nu_t(u_z+w_x)\}_z \\ &= \{\nu_t(u_x-v_y-w_z)\}_x + \{\nu_t(u_y+v_x)\}_y + \{\nu_t(u_z+w_x)\}_z \\ &= [J\nu_t\{(GG)u_\xi + (GE)u_\eta + (GC)u_\zeta - (z_\zeta/J)v_\eta + (z_\eta/J)v_\zeta + (y_\zeta/J)w_\eta - (y_\eta/J)w_\zeta\}]_\xi/J \\ &+ [J\nu_t\{(GE)u_\xi + (EE)u_\eta + (EC)u_\zeta + (z_\zeta/J)v_\xi - (z_\xi/J)v_\zeta - (y_\zeta/J)w_\xi + (y_\xi/J)w_\zeta\}]_\eta/J \\ &+ [J\nu_t\{(GC)u_\xi + (EC)u_\eta + (CC)u_\zeta - (z_\eta/J)v_\xi + (z_\xi/J)v_\eta + (y_\eta/J)w_\xi - (y_\xi/J)w_\eta\}]_\zeta/J \end{aligned} \tag{1.13}$$

here, GG, GE, GC, etc. are defined in Equation (1-23)

$$\begin{aligned} FY &= \{\nu_t(u_y+v_x)\}_x + \{\nu_t(2v_y)\}_y + \{\nu_t(v_z+w_y)\}_z \\ &= \{\nu_t(u_y+v_x)\}_x + \{\nu_t(v_y-u_x-w_z)\}_y + \{\nu_t(v_z+w_y)\}_z \\ &= [J\nu_t\{(GG)v_\xi + (GE)v_\eta + (GC)v_\zeta + (z_\zeta/J)u_\eta - (z_\eta/J)u_\zeta - (x_\zeta/J)w_\eta + (x_\eta/J)w_\zeta\}]_\xi/J \\ &+ [J\nu_t\{(GE)v_\xi + (EE)v_\eta + (EC)v_\zeta - (z_\zeta/J)u_\xi + (z_\xi/J)u_\zeta + (x_\zeta/J)w_\xi - (x_\xi/J)w_\zeta\}]_\eta/J \\ &+ [J\nu_t\{(GC)v_\xi + (EC)v_\eta + (CC)v_\zeta + (z_\eta/J)u_\xi - (z_\xi/J)u_\eta - (x_\eta/J)w_\xi + (x_\xi/J)w_\eta\}]_\zeta/J \end{aligned} \tag{1.14}$$

$$\begin{aligned} FZ &= \{\nu_t(w_x+u_z)\}_x + \{\nu_t(w_y+v_z)\}_y + \{\nu_t(2w_z)\}_z \\ &= \{\nu_t(w_x+u_z)\}_x + \{\nu_t(w_y+v_z)\}_y + \{\nu_t(w_z-u_x-v_y)\}_z \\ &= [J\nu_t\{(GG)w_\xi + (GE)w_\eta + (GC)w_\zeta - (y_\zeta/J)u_\eta + (y_\eta/J)u_\zeta + (x_\zeta/J)v_\eta - (x_\eta/J)v_\zeta\}]_\xi/J \\ &+ [J\nu_t\{(GE)w_\xi + (EE)w_\eta + (EC)w_\zeta + (y_\zeta/J)u_\xi - (y_\xi/J)u_\zeta - (x_\zeta/J)v_\xi + (x_\xi/J)v_\zeta\}]_\eta/J \\ &+ [J\nu_t\{(GC)w_\xi + (EC)w_\eta + (CC)w_\zeta - (y_\eta/J)u_\xi + (y_\xi/J)u_\eta + (x_\eta/J)v_\xi - (x_\xi/J)v_\eta\}]_\zeta/J \end{aligned} \tag{1.15}$$

TURBULENCE ENERGY k

Transport Equation of k

$$k_\tau + HK = FK + \nu_t S - \varepsilon \tag{1.16}$$

Convection Term of k

TABLE 1 (*Continued*)
Governing Equations of the k-ϵ Model with Generalized Curvilinear Coordinates

$$HK=(ku)_x+(kv)_y+(kw)_z$$
$$=\{(JUk)_\xi+(JVk)_\eta+(JWk)_\zeta\}/J \tag{1.17}$$

Diffusion Term of k

$$FK=(\nu_t k_x/\sigma_1)_x+(\nu_t k_y/\sigma_1)_y+(\nu_t k_z/\sigma_1)_z$$
$$=[J\nu_t\{(GG)k_\xi+(GE)k_\eta+(GC)k_\zeta\}/\sigma_1]_\xi/J$$
$$+[J\nu_t\{(GE)k_\xi+(EE)k_\eta+(EC)k_\zeta\}/\sigma_1]_\eta/J$$
$$+[J\nu_t\{(GC)k_\xi+(EC)k_\eta+(CC)k_\zeta\}/\sigma_1]_\zeta/J \tag{1.18}$$

Production Term

$$\nu_t S=\nu_t\{2u_x^2+2v_y^2+2w_z^2+(u_y+v_x)^2+(w_x+u_z)^2+(v_z+w_y)^2\}$$
$$=2\nu_t[\{(J\xi_x u)_\xi+(J\eta_x u)_\eta+(J\zeta_x u)_\zeta\}/J]^2$$
$$+2\nu_t[\{(J\xi_y v)_\xi+(J\eta_y v)_\eta+(J\zeta_y v)_\zeta\}/J]^2$$
$$+2\nu_t[\{(J\xi_z w)_\xi+(J\eta_z w)_\eta+(J\zeta_z w)_\zeta\}/J]^2$$
$$+\nu_t[\{(J\xi_y u+J\xi_x v)_\xi+(J\eta_y u+J\eta_x v)_\eta+(J\zeta_y u+J\zeta_x v)_\zeta\}/J]^2$$
$$+\nu_t[\{(J\xi_x w+J\xi_z u)_\xi+(J\eta_x w+J\eta_z u)_\eta+(J\zeta_x w+J\zeta_z u)_\zeta\}/J]^2$$
$$+\nu_t[\{(J\xi_z v+J\xi_y w)_\xi+(J\eta_z v+J\eta_y w)_\eta+(J\zeta_z v+J\zeta_y w)_\zeta\}/J]^2 \tag{1.19}$$

DISSIPATION RATE ϵ

Transportation Equation of ϵ

$$\epsilon_t+HE=FE+c_1\epsilon\nu_t S/k-c_2\epsilon^2/k \tag{1.20}$$

Convection Term of ϵ

TABLE 1 (*Concluded*)
Governing Equations of the k-ϵ Model with Generalized Curvilinear Coordinates

$$HE=(\varepsilon u)_x+(\varepsilon v)_y+(\varepsilon w)_z$$
$$=\{(JU\varepsilon)_\xi+(JV\varepsilon)_\eta+(JW\varepsilon)_\zeta\}/J \tag{1.21}$$

Diffusion Term of ε

$$FE=(\nu_t\varepsilon_x/\sigma_2)_x+(\nu_t\varepsilon_y/\sigma_2)_y+(\nu_t\varepsilon_z/\sigma_2)_z$$
$$=[J\nu_t\{(GG)\varepsilon_\xi+(GE)\varepsilon_\eta+(GC)\varepsilon_\zeta\}/\sigma_2]_\xi/J$$
$$+[J\nu_t\{(GE)\varepsilon_\xi+(EE)\varepsilon_\eta+(EC)\varepsilon_\zeta\}/\sigma_2]_\eta/J$$
$$+[J\nu_t\{(GC)\varepsilon_\xi+(EC)\varepsilon_\eta+(CC)\varepsilon_\zeta\}/\sigma_2]_\zeta/J \tag{1.22}$$

where

$$GG=\xi_x^2+\xi_y^2+\xi_z^2, \qquad EE=\eta_x^2+\eta_y^2+\eta_z^2,$$
$$CC=\zeta_x^2+\zeta_y^2+\zeta_z^2, \qquad GE=\xi_x\eta_x+\xi_y\eta_y+\xi_z\eta_z,$$
$$GC=\xi_x\zeta_x+\xi_y\zeta_y+\xi_z\zeta_z, \quad EC=\eta_x\zeta_x+\eta_y\zeta_y+\eta_z\zeta_z \tag{1.23}$$

$$J=\begin{vmatrix} x_\xi & x_\eta & x_\zeta \\ y_\xi & y_\eta & y_\zeta \\ z_\xi & z_\eta & z_\zeta \end{vmatrix}=\begin{vmatrix} \xi_x & \xi_y & \xi_z \\ \eta_x & \eta_y & \eta_z \\ \zeta_x & \zeta_y & \zeta_z \end{vmatrix}^{-1}$$

$$\xi_x=(y_\eta z_\zeta-y_\zeta z_\eta)/J,\ \xi_y=-(x_\eta z_\zeta-x_\zeta z_\eta)/J,\ \xi_z=(x_\eta y_\zeta-x_\zeta y_\eta)/J,$$
$$\eta_x=-(y_\xi z_\zeta-y_\zeta z_\xi)/J,\ \eta_y=(x_\xi z_\zeta-x_\zeta z_\xi)/J,\ \eta_z=-(x_\xi y_\zeta-x_\zeta y_\xi)/J,$$
$$\zeta_x=(y_\xi z_\eta-y_\eta z_\xi)/J,\ \zeta_y=-(x_\xi z_\eta-x_\eta z_\xi)/J,\ \zeta_z=(x_\xi y_\eta-x_\eta y_\xi)/J,$$
$$x_\xi=J(\eta_y\zeta_z-\zeta_y\eta_z),\ x_\eta=-J(\xi_y\zeta_z-\zeta_y\xi_z),\ x_\zeta=J(\xi_y\eta_z-\eta_y\xi_z),$$
$$y_\xi=-J(\eta_x\zeta_z-\zeta_x\eta_z),\ y_\eta=J(\xi_x\zeta_z-\zeta_x\xi_z),\ y_\zeta=-J(\xi_x\eta_z-\eta_x\xi_z),$$
$$z_\xi=J(\eta_x\zeta_y-\zeta_x\eta_y),\ z_\eta=-J(\xi_x\zeta_y-\zeta_x\xi_y),\ z_\zeta=J(\xi_x\eta_y-\eta_x\xi_y) \tag{1.24}$$

DEFINITION OF ν_t

$$\nu_t=k^{1/2}l=c_Dk^2/\varepsilon \tag{1.25}$$

EMPIRICAL CONSTANTS

$$\sigma_1=1.0,\ \sigma_2=1.3,\ c_D=0.09,\ c_1=1.44,\ c_2=1.92 \tag{1.26}$$

TABLE 2
Boundary Conditions of Velocity and Turbulence Properties

Constant ξ Surface

Velocity Gradients at Wall

Based on the Power Law Distribution of Tangential Velocity near Wall

$$(u_\ell^{t\ell\eta})_{i,j,k}$$

$$= \{(m/h)(u^{t\ell\eta})_{i,j,k}\}/(GG)^{1/2} - \{(GE)(u_\eta^{t\ell\eta})_{i,j,k} + (GC)(u_\ell^{t\ell\eta})_{i,j,k}\}/(GG) \tag{2.1}$$

$$(u_\ell^{t\ell\zeta})_{i,j,k}$$

$$= \{(m/h)(u^{t\ell\zeta})_{i,j,k}\}/(GG)^{1/2} - \{(GE)(u_\eta^{t\ell\zeta})_{i,j,k} + (GC)(u_\ell^{t\ell\zeta})_{i,j,k}\}/(GG) \tag{2.2}$$

$$(u_\ell)_{i,j,k}$$

$$= \{-(y_\eta\xi_z - z_\eta\xi_y)(x_\ell^2+y_\ell^2+z_\ell^2)^{1/2}(u_\ell^{t\ell\eta})_{i,j,k} + (y_\ell\xi_z - z_\ell\xi_y)(x_\eta^2+y_\eta^2+z_\eta^2)^{1/2}(u_\ell^{t\ell\zeta})_{i,j,k}$$
$$+ J\xi_x(C^\ell)_{i,j,k}\}/\{J(GG)\} \tag{2.3}$$

$$(v_\ell)_{i,j,k}$$

$$= \{(x_\eta\xi_z - z_\eta\xi_x)(x_\ell^2+y_\ell^2+z_\ell^2)^{1/2}(u_\ell^{t\ell\eta})_{i,j,k} - (x_\ell\xi_z - z_\ell\xi_x)(x_\eta^2+y_\eta^2+z_\eta^2)^{1/2}(u_\ell^{t\ell\zeta})_{i,j,k}$$
$$+ J\xi_y(C^\ell)_{i,j,k}\}/\{J(GG)\} \tag{2.4}$$

$$(w_\ell)_{i,j,k}$$

$$= \{-(x_\eta\xi_y - y_\eta\xi_x)(x_\ell^2+y_\ell^2+z_\ell^2)^{1/2}(u_\ell^{t\ell\eta})_{i,j,k} + (x_\ell\xi_y - y_\ell\xi_x)(x_\eta^2+y_\eta^2+z_\eta^2)^{1/2}(u^t\xi^\zeta)_{i,j,k}$$
$$+ J\xi_z(C^\ell)_{i,j,k}\}/\{J(GG)\} \tag{2.5}$$

$$C^\ell = -\{\eta_x u_\eta + \eta_y v_\eta + \eta_z w_\eta + \zeta_x u_\ell + \zeta_y v_\ell + \zeta_z w_\ell\} \tag{2.6}$$

Free Slip Condition of k

$$\int_{s1}[\{J\nu_t(\xi_x k_x + \xi_y k_y + \xi_z k_z)\}/\sigma_1]\,d\eta\,d\zeta = \int_{s1}[\{J\nu_t(\xi_x^2+\xi_y^2+\xi_z^2)^{1/2}(\partial k/\partial N)\}/\sigma_1]\,d\eta\,d\zeta = 0 \tag{2.7}$$

TABLE 2 (*Continued*)
Boundary Conditions of Velocity and Turbulence Properties

where N is a normal distance measured from the physical boundary surface, h is a normal distance between the physical surface and the computational one and κ is the Karman constant, 0.4.

Constant η Surface

Velocity Gradients at Wall

Based on the Power Law Distribution of Tangential Velocity near Wall

$$(u_\eta^{t\eta\ell})_{i,j,k}$$
$$=\{(m/h)(u^{t\eta\ell})_{i,j,k}\}/(EE)^{1/2}-\{(GE)(u_\ell^{t\eta\ell})_{i,j,k}+(EC)(u_\ell^{t\eta\ell})_{i,j,k}\}/(EE) \quad (2.8)$$

$$(u_\eta^{t\eta\ell})_{i,j,k}$$
$$=\{(m/h)(u^{t\eta\ell})_{i,j,k}\}/(EE)^{1/2}-\{(GE)(u_\ell^{t\eta\ell})_{i,j,k}+(EC)(u_\ell^{t\eta\ell})_{i,j,k}\}/(EE) \quad (2.9)$$

$$(u_\eta)_{i,j,k}$$
$$=\{(y_\ell\eta_z-z_\ell\eta_y)(x_\ell^2+y_\ell^2+z_\ell^2)^{1/2}(u_\eta^{t\eta\ell})_{i,j,k}-(y_\ell\eta_z-z_\ell\eta_y)(x_\ell^2+y_\ell^2+z_\ell^2)^{1/2}(u^{t\eta\ell})_{i,j,k}$$
$$+J\eta_x(C^\eta)_{i,j,k}\}/\{J(EE)\} \quad (2.10)$$

$$(y_\eta)_{i,j,k}$$
$$=\{-(x_\ell\eta_z-z_\ell\eta_x)(x_\ell^2+y_\ell^2+z_\ell^2)^{1/2}(u_\eta^{t\eta\ell})_{i,j,k}+(x_\ell\eta_z-z_\ell\eta_x)(x_\ell^2+y_\ell^2+z_\ell^2)^{1/2}(u_\eta^{t\eta\ell})_{i,j,k}$$
$$+J\eta_y(C^\eta)_{i,j,k}\}/\{J(EE)\} \quad (2.11)$$

$$(w_\eta)_{i,j,k}$$
$$=\{(x_\ell\eta_y-y_\ell\eta_x)(x_\ell^2+y_\ell^2+z_\ell^2)^{1/2}(u_\eta^{t\eta\ell})_{i,j,k}-(x_\ell\eta_y-y_\ell\eta_x)(x_\ell^2+y_\ell^2+z_\ell^2)^{1/2}(u_\eta^{t\eta\ell})_{i,j,k}$$
$$+J\eta_z(C^\eta)_{i,j,k}\}/\{J(EE)\} \quad (2.12)$$

$$C^\eta=-\{\xi_x u_\ell+\xi_y v_\ell+\xi_z w_\ell+\zeta_x u_\ell+\zeta_y v_\ell+\zeta_z w_\ell\} \quad (2.13)$$

Free Slip Condition of k

$$\int_{s3}[\{J\nu_t(\eta_x k_x+\eta_y k_y+\eta_z k_z)\}/\sigma_1]\,d\eta\,d\zeta=\int_{s1}[\{J\nu_t(\eta_x^2+\eta_y^2+\eta_z^2)^{1/2}(\partial k/\partial N)\}/\sigma_1]\,d\xi\,d\zeta=0 \quad (2.14)$$

TABLE 2 (*Concluded*)
Boundary Conditions of Velocity and Turbulence Properties

Constant ζ Surface

Velocity Gradients at Wall

Based on the Power Law Distribution of Tangential Velocity near Wall

$$(u_\ell^{t\ell\ell})_{i,j,k}$$

$$= \{(m/h)(u^{t\ell\ell})_{i,j,k}\}/(EE)^{1/2} - \{(GC)(u_\ell^{t\ell\ell})_{i,j,k} + (EC)(u_\eta^{t\ell\ell})_{i,j,k}\}/(EE) \tag{2.15}$$

$$(u_\ell^{t\ell\eta})_{i,j,k}$$

$$= \{(m/h)(u^{t\ell\eta})_{i,j,k}\}/(CC)^{1/2} - \{(GC)(u_\ell^{t\ell\eta})_{i,j,k} + (EC)(u_\eta^{t\ell\eta})_{i,j,k}\}/(CC) \tag{2.16}$$

$$(u_\ell)_{i,j,k}$$

$$= \{-(y_\ell\zeta_z - z_\ell\zeta_y)(x_\eta^2+y_\eta^2+z_\eta^2)^{1/2}(u_\ell^{t\ell\ell})_{i,j,k} + (y_\eta\zeta_z - z_\eta\zeta_y)(x_\ell^2+y_\ell^2+z_\ell^2)^{1/2}(u_\ell^{t\ell\eta})_{i,j,k}$$
$$+ J\zeta_x(C^t)_{i,j,k}\}/\{J(CC)\} \tag{2.17}$$

$$(v_\ell)_{i,j,k}$$

$$= \{(x_\ell\zeta_z - z_\ell\zeta_x)(x_\eta^2+y_\eta^2+z_\eta^2)^{1/2}(u_\ell^{t\ell\ell})_{i,j,k} - (x_\eta\zeta_z - z_\eta\zeta_x)(x_\ell^2+y_\ell^2+z_\ell^2)^{1/2}(u_\ell^{t\ell\eta})_{i,j,k}$$
$$+ J\zeta_y(C^t)_{i,j,k}\}/\{J(CC)\} \tag{2.18}$$

$$(w_\ell)_{i,j,k}$$

$$= \{-(x_\ell\zeta_y - y_\ell\zeta_x)(x_\eta^2+y_\eta^2+z_\eta^2)^{1/2}(u_\ell^{t\ell\ell})_{i,j,k} + (x_\eta\zeta_y - y_\eta\zeta_x)(x_\ell^2+y_\ell^2+z_\ell^2)^{1/2}(u_\ell^{t\ell\eta})_{i,j,k}$$
$$+ J\zeta_z(C^t)_{i,j,k}\}/\{J(CC)\} \tag{2.19}$$

$$C^t = -\{\zeta_x u_\ell + \zeta_y v_\ell + \zeta_z w_\ell + \eta_x u_\eta + \eta_y v_\eta + \eta_z w_\eta\} \tag{2.20}$$

Free Slip Condition of k

$$\int_{s_2}^{s_3}[\{J\nu_t(\zeta_x k_x + \zeta_y k_y + \zeta_z k_z)\}/\sigma_1]\,d\eta\,d\zeta = \int_{s_1}^{s_2}[\{J\nu_t(\zeta_x^2+\zeta_y^2+\zeta_z^2)^{1/2}(\partial k/\partial N)\}/\sigma_1]\,d\xi\,d\eta = 0 \tag{2.21}$$

Wall Law of ε

$$\varepsilon_{i,j,k} = \{C_D^{3/4}/(\kappa h)\}\,k_{i,j,k}^{3/2} \tag{2.22}$$

here, κ = von Karman constant, $\kappa = 0.4$

TABLE 3
Poisson Equation and Generation Term

POISSON EQUATION OF PRESSURE

$$
\begin{aligned}
&L_2\,[\{J(GG)\}_{i+1/2,j,k}(p_{i+1,j,k}-p_{i,j,k})+\{J(GE)\}_{i+1,j,k}(p_{i+1,j+1,k}-p_{i+1,j-1,k})/4\\
&\quad+\underline{\{J(GE)\}_{i,j,k}(p_{i,j+1,k}-p_{i,j-1,k})/4}+\{J(GC)\}_{i+1,j,k}(p_{i+1,j,k+1}-p_{i+1,j,k-1})/4\\
&\quad+\underline{\{J(GC)\}_{i,j,k}(p_{i,j,k+1}-p_{i,j,k-1})/4}]\\
&-L_1\,[\{J(GG)\}_{i-1/2,j,k}(p_{i,j,k}-p_{i-1,j,k})+\{J(GE)\}_{i-1,j,k}(p_{i-1,j+1,k}-p_{i-1,j-1,k})/4\\
&\quad+\underline{\{J(GE)\}_{i,j,k}(p_{i,j+1,k}-p_{i,j-1,k})/4}+\{J(GC)\}_{i-1,j,k}(p_{i-1,j,k+1}-p_{i-1,j,k-1})/4\\
&\quad+\underline{\{J(GC)\}_{i,j,k}(p_{i,j,k+1}-p_{i,j,k-1})/4}]\\
&+L_4\,[\{J(GE)\}_{i,j+1,k}(p_{i+1,j+1,k}-p_{i-1,j+1,k})/4+\underline{\{J(GE)\}_{i,j,k}(p_{i+1,j,k}-p_{i-1,j,k})/4}\\
&\quad+\{J(EE)\}_{i,j+1/2,k}(p_{i,j+1,k}-p_{i,j,k})+\{J(EC)\}_{i,j+1,k}(p_{i,j+1,k+1}-p_{i,j+1,k-1})/4\\
&\quad+\underline{\{J(EC)\}_{i,j,k}(p_{i,j,k+1}-p_{i,j,k-1})/4}]\\
&-L_3\,[\{J(GE)\}_{i,j-1,k}(p_{i+1,j-1,k}-p_{i-1,j-1,k})/4+\underline{\{J(GE)\}_{i,j,k}(p_{i+1,j,k}-p_{i-1,j,k})/4}\\
&\quad+\{J(EE)\}_{i,j-1/2,k}(p_{i,j,k}-p_{i,j-1,k})+\{J(EC)\}_{i,j-1,k}(p_{i,j-1,k+1}-p_{i,j-1,k-1})/4\\
&\quad+\underline{\{J(EC)\}_{i,j,k}(p_{i,j,k+1}-p_{i,j,k-1})/4}]\\
&+L_6\,[\{J(GC)\}_{i,j,k+1}(p_{i+1,j,k+1}-p_{i-1,j,k+1})/4+\underline{\{J(GC)\}_{i,j,k}(p_{i+1,j,k}-p_{i-1,j,k})/4}\\
&\quad+\{J(EC)\}_{i,j,k+1}(p_{i,j+1,k+1}-p_{i,j-1,k+1})/4+\underline{\{J(EC)\}_{i,j,k}(p_{i,j+1,k}-p_{i,j-1,k})/4}\\
&\quad+\{J(CC)\}_{i,j,k+1/2}(p_{i,j,k+1}-p_{i,j,k})]\\
&-L_5\,[\{J(GC)\}_{i,j,k-1}(p_{i+1,j,k-1}-p_{i-1,j,k-1})/4+\underline{\{J(GC)\}_{i,j,k}(p_{i+1,j,k}-p_{i-1,j,k})/4}\\
&\quad+\{J(EC)\}_{i,j,k-1}(p_{i,j+1,k-1}-p_{i,j-1,k-1})/4+\underline{\{J(EC)\}_{i,j,k}(p_{i,j+1,k}-p_{i,j-1,k})/4}\\
&\quad+J(CC)_{i,j,k-1/2}(p_{i,j,k}-p_{i,j,k-1})]
\end{aligned}
\tag{3.1}
$$

$$=\tilde{D}/\Delta t,$$

where underlined terms vanish when all of $L_{1\sim6}$ equals unity.

Generation Term

$$\tilde{D}=-\int_{s1}\{J\tilde{U}\}\,d\eta\,d\zeta+\int_{s2}\{J\tilde{U}\}\,d\eta\,d\zeta-\int_{s3}\{J\tilde{V}\}\,d\xi\,d\zeta+\int_{s4}\{J\tilde{V}\}\,d\xi\,d\zeta-\int_{s5}\{J\tilde{W}\}\,d\xi\,d\eta+\int_{s6}\{J\tilde{W}\}\,d\xi\,d\eta \tag{3.2}$$

Discrete Expression for Full Control Volume

TABLE 3 (*Concluded*)
Poisson Equation and Generation Term

$$\tilde{D}=\{(J\tilde{U})_{i+1,j,k}-(J\tilde{U})_{i-1,j,k}+(J\tilde{V})_{i,j+1,k}-(J\tilde{V})_{i,j-1,k}+(J\tilde{W})_{i,j,k+1}-(J\tilde{W})_{i,j,k-1}\}/2 \tag{3.3}$$

Discrete Expression for One-half Control Volume

$$\tilde{D}=\{(J\tilde{U})_{i+1,j,k}-(J\tilde{U})_{i,j,k}\}/2+\{(J\tilde{V})_{i,j+1,k}-(J\tilde{V})_{i,j-1,k}+(J\tilde{W})_{i,j,k+1}-(J\tilde{W})_{i,j,k-1}\}/4 \tag{3.4}$$

Definition of L_i

$L_1=I_1(I_3+I_4)(I_5+I_6)/4$, $L_2=I_2(I_3+I_4)(I_5+I_6)/4$, $L_3=I_3(I_1+I_2)(I_5+I_6)/4$,
$L_4=I_4(I_1+I_2)(I_5+I_6)/4$, $L_5=I_5(I_1+I_2)(I_3+I_4)/4$, $L_6=I_6(I_1+I_2)(I_3+I_3)/4$,
I_i =0 : if the surface S_i coincides with the boundary,
=1 : if the surface S_i does not coincide with the boundary. (3.5)

Definitions of $\tilde{U}$, $\tilde{V}$, and $\tilde{W}$

If each surface of the control volume does not coincide with the boundary,

$\tilde{U}=(\xi_x,\xi_y,\xi_z)\cdot\{(u,v,w)^{n}+\Delta t(-HX+FX,-HY+FY,-HZ+FZ)^{n+1}\}$ (constant ξ surface),

$\tilde{V}=(\eta_x,\eta_y,\eta_z)\cdot\{(u,v,w)^{n}+\Delta t(-HX+FX,-HY+FY,-HZ+FZ)^{n+1}\}$ (constant η surface),

$\tilde{W}=(\zeta_x,\zeta_y,\zeta_z)\cdot\{(u,v,w)^{n}+\Delta t(-HX+FX,-HY+FY,-HZ+FZ)^{n+1}\}$ (constant ζ surface). (3.6)

If each surface of the control volume coincides with the boundary, respectively,

$\tilde{U}$=U(constant ξ surface),

$\tilde{V}$=V(constant η surface),

$\tilde{W}$=W(constant ζ surface). (3.7)

TABLE 4
Relaxation Equations

RELAXATION EQUATIONS FOR VELOCITY COMPONENTS

$$ {}^{\ell+1}u_{i,j,k}^{n+1} = {}^{\ell}u_{i,j,k}^{n+1} + \omega^{u} c^{u} \tag{4.1} $$

$$ {}^{\ell+1}v_{i,j,k}^{n+1} = {}^{\ell}v_{i,j,k}^{n+1} + \omega^{u} c^{v} \tag{4.2} $$

$$ {}^{\ell+1}w_{i,j,k}^{n+1} = {}^{\ell}w_{i,j,k}^{n+1} + \omega^{u} c^{w} \tag{4.3} $$

Correction Values

$$ c^{u} = (x_{\xi} e^{U} I^{i} + x_{\eta} e^{V} I^{j} + x_{\zeta} e^{W} I^{k}) / \{1 + (\Delta t / J_{i,j,k}) PVT_{i,j,k}\} $$

$$ c^{v} = (y_{\xi} e^{U} I^{i} + y_{\eta} e^{V} I^{j} + y_{\zeta} e^{W} I^{k}) / \{1 + (\Delta t / J_{i,j,k}) PVT_{i,j,k}\} $$

$$ c^{w} = (z_{\xi} e^{U} I^{i} + z_{\eta} e^{V} I^{j} + z_{\zeta} e^{W} I^{k}) / \{1 + (\Delta t / J_{i,j,k}) PVT_{i,j,k}\} \tag{4.4} $$

Error Values of Contravariant Vector Components

$$ e^{U} = \xi_{x} e^{u} + \xi_{y} e^{v} + \xi_{z} e^{w}, \quad e^{V} = \eta_{x} e^{u} + \eta_{y} e^{v} + \eta_{z} e^{w}, \quad e^{W} = \zeta_{x} e^{u} + \zeta_{y} v^{v} + \zeta_{z} e^{w} \tag{4.5} $$

Error Values of Velocity Vector Components

$$ e^{u} = -{}^{\ell}u^{n+1} + u^{n} + (\Delta t / J) \int_{V} \{ -{}^{\ell}p_{x}^{n+1} - {}^{\ell}HX^{n+1} + {}^{\ell}FX^{n+1} \} dV $$

$$ e^{v} = -{}^{\ell}v^{n+1} + v^{n} + (\Delta t / J) \int_{V} \{ -{}^{\ell}p_{y}^{n+1} - {}^{\ell}HY^{n+1} + {}^{\ell}FY^{n+1} \} dV $$

$$ e^{w} = -{}^{\ell}w^{n+1} + w^{n} + (\Delta t / J) \int_{V} \{ -{}^{\ell}p_{z}^{n+1} - {}^{\ell}HZ^{n+1} + {}^{\ell}FZ^{n+1} \} dV \tag{4.6} $$

Definition of I^{i}, I^{j}, and I^{k}

If a surface of the control volume coincides with the boundary:

$I^{i} = 0$ (constant ξ surface),

$I^{j} = 0$ (constant η surface),

$I^{k} = 0$ (constant ζ surface),

If a surface of the control volume does not coincide with the boundary:

$I^{i} = 1$ (constant ξ surface),

$I^{j} = 1$ (constant η surface),

$I^{k} = 1$ (constant ζ surface), (4.7)

TABLE 4
Relaxation Equations (*Concluded*)

Pivot Value of Relaxation

: Diagonal Term of Coefficient Matrices of Simultaneous Equations for u, v, w, k, and ε

$$
\begin{aligned}
&PVT_{i,j,k} \\
&= [\{J_{\nu_t}(GG)\}_{i,j,k} + \{J_{\nu_t}(GG)\}_{i+1,j,k}]\, I^{i+1/2}/2 \\
&+ [\{J_{\nu_t}(GG)\}_{i,j,k} + \{J_{\nu_t}(GG)\}_{i-1,j,k}]\, I^{i-1/2}/2 \\
&+ [\{J_{\nu_t}(EE)\}_{i,j,k} + \{J_{\nu_t}(EE)\}_{i,j+1,k}]\, I^{j+1/2}/2 \\
&+ [\{J_{\nu_t}(EE)\}_{i,j,k} + \{J_{\nu_t}(EE)\}_{i,j-1,k}]\, I^{j-1/2}/2 \\
&+ [\{J_{\nu_t}(CC)\}_{i,j,k} + \{J_{\nu_t}(CC)\}_{i,j,k+1}]\, I^{k+1/2}/2 \\
&+ [\{J_{\nu_t}(CC)\}_{i,j,k} + \{J_{\nu_t}(CC)\}_{i,j,k-1}]\, I^{k-1/2}/2 \qquad (4.8)
\end{aligned}
$$

If $\{(i-1/2).GT.0$ .and. $(i+1/2).LT.i_{max}\}$ $I^{i\pm1/2}=1$

If $\{(i-1/2).LT.0\}$ $I^{i-1/2}=0.$

If $\{(i+1/2).GT.i_{max}\}$ $I^{i+1/2}=0.$ (4.9)

Same conditions are applied to $I^{j\pm1/2}$ and $I^{k\pm1/2}$.

RELAXATION EQUATION FOR k

$$
\begin{aligned}
{}^{t+1}k_{i,j,k}{}^{n+1} = {}^{t}k_{i,j,k}{}^{n+1} + \omega^k [&-{}^{t}k^{n+1} + k^n + (\Delta t/J)/_V \{-{}^{t}HK^{n+1} + {}^{t}FK^{n+1}\}\, dV \\
&+ \Delta t \{{}^{t}\nu_t{}^{n+1}\, S^{n+1} - {}^{t}\varepsilon^{n+1}\}]_{i,j,k} / \{1 + (\Delta t/J_{i,j,k})(PVT_{i,j,k}/\sigma_1)\} \qquad (4.10)
\end{aligned}
$$

RELAXATION EQUATION FOR ε

$$
\begin{aligned}
{}^{t+1}\varepsilon_{i,j,k}{}^{n+1} = {}^{t}\varepsilon_{i,j,k}{}^{n+1} + \omega' [&-{}^{t}\varepsilon^{n+1} + \varepsilon^n + (\Delta t/J)/_V \{-{}^{t}HE^{n+1} + {}^{t}FE^{n+1}\}\, dV \\
&+ \Delta t \{c_1 {}^{t}\varepsilon^{n+1}\, {}^{t}\nu_t{}^{n+1}\, S^{n+1}/{}^{t}k^{n+1} - c_2 ({}^{t}\varepsilon^{n+1})^2/{}^{t}k^{n+1}\}]_{i,j,k} \\
/\, [1 - \Delta t \{c_1 {}^{t}\nu_t{}^{n+1}\, S^{n+1}/{}^{t}k^{n+1} - c_2 {}^{t}\varepsilon^{n+1}/{}^{t}k^{n+1}\} + (\Delta t/J_{i,j,k})(PVT_{i,j,k}/\sigma_2)] \qquad (4.11)
\end{aligned}
$$

RELAXATION EQUATION FOR PRESSURE

$$
\begin{aligned}
{}^{t+1}p_{i,j,k}{}^{n+1} = {}^{t}p_{i,j,k}{}^{n+1} + \omega^p [&/_V \{p_{xx}{}^{n+1} + p_{yy}{}^{n+1} + p_{zz}{}^{n+1} - (u_x + v_y + w_z)^n/\Delta t \\
&- (-HX_x - HY_x - HZ_y + FX_y + FY_z + FZ_z)^{n+1}\}\, dV]_{i,j,k} / PVP_{i,j,k} \qquad (4.12)
\end{aligned}
$$

where $\omega^u, \omega^k, \omega', \omega^p$ are over/under relaxation factors.

The equation of PVP can be derived by substituting the unity value of ν_t into Equation 4.8.

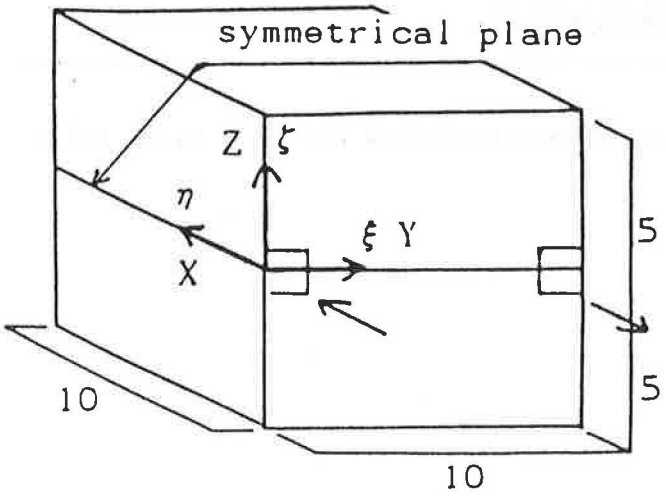

Figure 2 *Room model*

dices. The governing equations of the k-ϵ model with the generalized curvilinear coordinates are expressed in Table 1. Boundary conditions of velocity and turbulence properties are shown in Table 2. The discretized Poisson equation and its generation term are represented in Table 3. The relaxation equations are shown in Table 4 and its procedure is illustrated in Figure 23.

APPLICATION TO ROOM AIRFLOW

Comparison of Numerical to Experimental Results Based on Cubic-Shaped Room Model

The authors compare the results of the present numerical method, based on the generalized curvilinear system, with the preceding ordinary numerical study in order to confirm the applicability of this method. The latter results are not based on the generalized curvilinear coordinates.

In an earlier study (Nomura et al. 1980), the room airflow in a cubic-shaped room was precisely measured three-dimensionally and a numerical simulation based on the k-ϵ model with Cartesian coordinates was conducted using a 20 x 20 x 20 staggered grid system of the MAC (marker and cell) method (Harlow et al. 1965); these were the prototypes for our latest numerical method (Murakami et al. 1987). The room model used for both the experimental and the numerical studies is shown in Figure 2. The model scale is normalized by the width of the square outlet. The velocity is normaiized by the supply outlet velocity.

We conducted a simulation by means of the k-ϵ model based on the present method using two types of grid discretizations: type 1 (20 × 20 × 20), which is shown in Figure 3, and type 2 (28 × 19 × 29), which is shown in Figures 4a, 4b, and 4c. The boundary conditions are described in detail in Table 5.

Figure 5 shows the distribution of the velocity vectors at the symmetrical plane, namely the η-ζ plane or the x-y plane. The results of the present method, shown in Figures 5c and 5d, agree well with the authors' experimental results of Figures 5a and with the numerical results based on the ordinary rectangular grid of Figure 5b. Figure 5e is an enlargement of the distribution of the velocity vectors around the vicinity of the exhaust inlet. The flow pattern is very smooth. The numerical instability, often observed in preceding studies, does not appear because of the fine grid discretization given by the generalized curvilinear coordinate system.

The turbulence kinetic energy, k, the turbulence dissipation rate, ϵ, and eddy viscosity, ν_t are shown in Figure 6. The effect of the coarseness of the discretization does not seem to be great, but some difference appears at the right-hand side of the supply jet region. it is observed that the gradients of k, ϵ, *and* ν_t are steeper at the jet region in Figure 6b (type 2) than those in Figure 6a (type 1). This difference is due to the fact that simulation with the finer grid can reproduce the velocity gradients more

The definition of the open area in the case of grid Type 1 is illustrated here. There is a small difference between the inflow rate of grid Type 1 and that of experiment. Detail are described in Table 5.

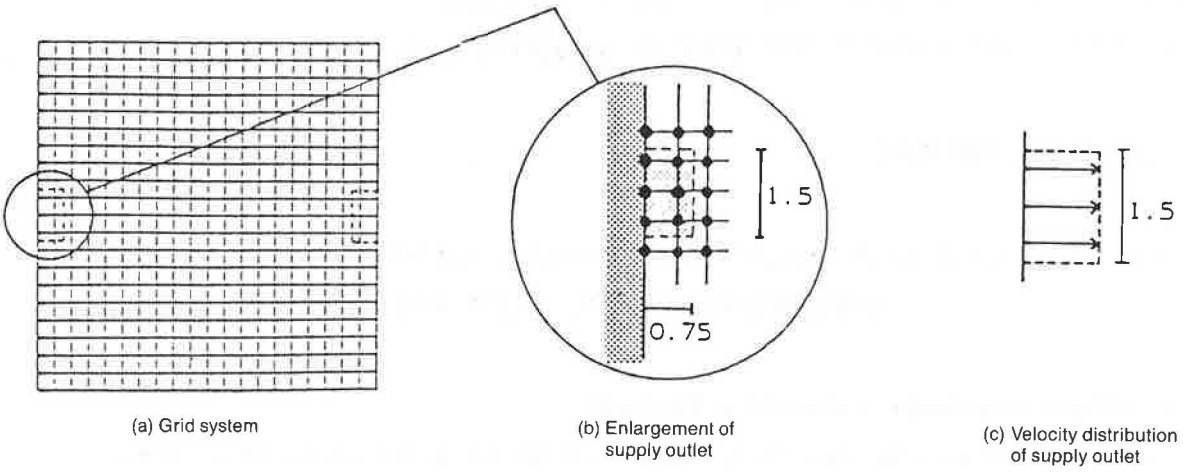

(a) Grid system

(b) Enlargement of supply outlet

(c) Velocity distribution of supply outlet

Figure 3 *Grid discretization of Type 1 (length scale and velocity scale are normalized by the width of the supply opening and the supply velocity, respectively)*

TABLE 5
Boundary Condition of Cubic-shaped Room Model

Supply outlet : $u^n=1.0$, $u^t=0.0$, $k=0.005$, $\ell=0.1$

Exhaust inlet : $u^n=1.0$, u^t, k, ε: free-slip

here, u^n is velocity component normal to outlet or inlet, and

u^t is velocity component tangential to outlet or inlet.

Wall boundary (wall) : $m=1/7$

(eight vertexes of the cubic room) : $u=v=w=0$

Time increment (grid type 1) : $\Delta t=0.1$

Time increment (grid type 2) : $\Delta t=0.05$

Distance between physical wall and computational boundary : $h=0.02$

Relaxation factors (in the vicinity of the exhaust inlet)

(grid type 1) : $\omega^p=\omega^u=0.5$, $\omega^k=\omega'=1.0$

(grid type 2) : $\omega^p=\omega^u=0.25$, $\omega^k=\omega'=1.0$

Relaxation factors (in the other region)

(grid type 1) : $\omega^p=\omega^u=1.0$, $\omega^k=\omega'=1.0$

(grid type 2) : $\omega^p=\omega^u=0.5$, $\omega^k=\omega'=1.0$

* Representative values for normalization : supply velocity, $U_o=1.0$ m/sec,
width of supply outlet, $L_o=1.0$ m

Note: Figure 3 b shows the definition of the open area at supply outlet of type 1. As for the definition of the inflow rate, there is a small difference between the regular grid system here and the staggered one of the preceding study. The inflow velocity distribution of grid type 1 at the supply opening is shown in Figure 3 c with a broken line. The distribution of the normal velocity component at the exhaust opening is similar to that at the supply opening. Due to the uniform grid arrangement, the open area of the supply outlet or the exhaust inlet does not agree with that of the experimental model 1.0×1.0. They are assumed here to be 1.5×0.75 for grid type 1 and 1.0×1.0 in experiment, as shown in Figure 3 b. But the velocity value is the same as the experimental value. The small difference in inflow rate has little influence on the entire flow field. Therefore, it may be regarded that same inflow condition is imposed on both simulation of grid type 1 and experiment.

In the discretization of type 2, the grid size for the open area can be adjusted to agree with that of the experimental model.

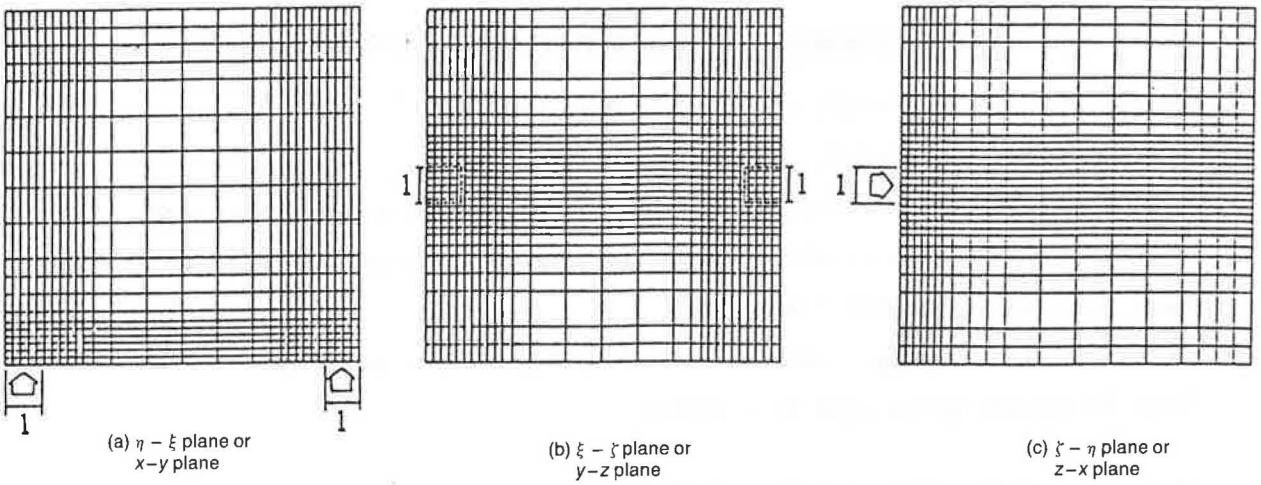

(a) $\eta - \xi$ plane or $x-y$ plane

(b) $\xi - \zeta$ plane or $y-z$ plane

(c) $\zeta - \eta$ plane or $z-x$ plane

Figure 4 *Grid discretization of Type 2*

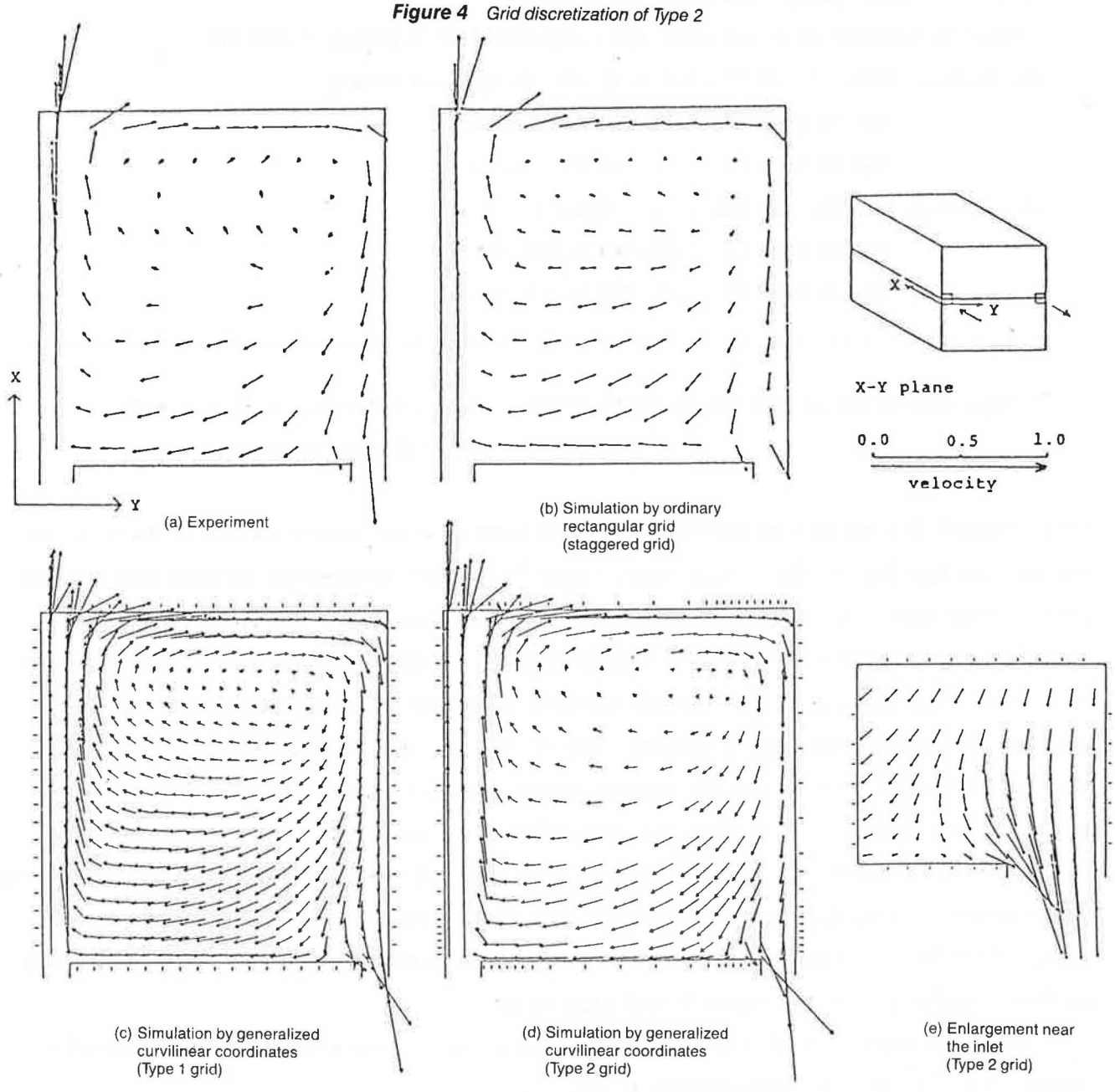

(a) Experiment

(b) Simulation by ordinary rectangular grid (staggered grid)

(c) Simulation by generalized curvilinear coordinates (Type 1 grid)

(d) Simulation by generalized curvilinear coordinates (Type 2 grid)

(e) Enlargement near the inlet (Type 2 grid)

Figure 5 *Comparison of velocity distribution*

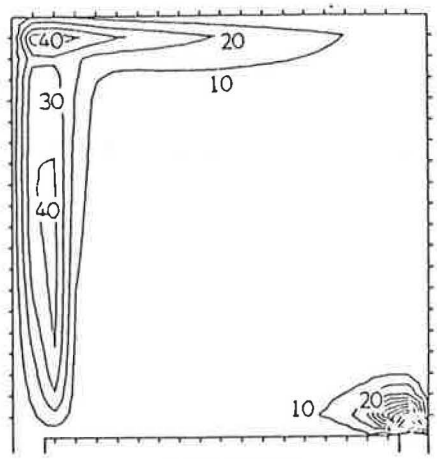

($k \times 10^{-3}$)

k Distribution

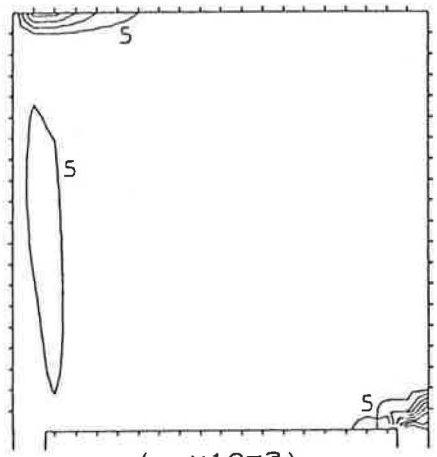

($\varepsilon \times 10^{-3}$)

ε Distribution

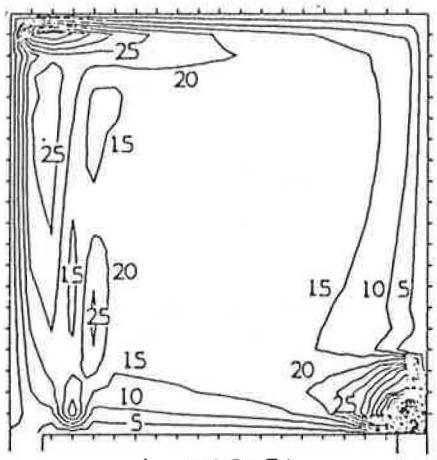

($\nu_t \times 10^{-3}$)

ν_t Distribution

(a) Plan of Tokyo gymnasium and quarter area used for simulation

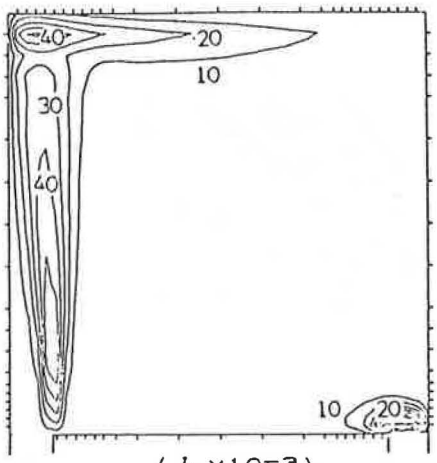

($k \times 10^{-3}$)

k Distribution

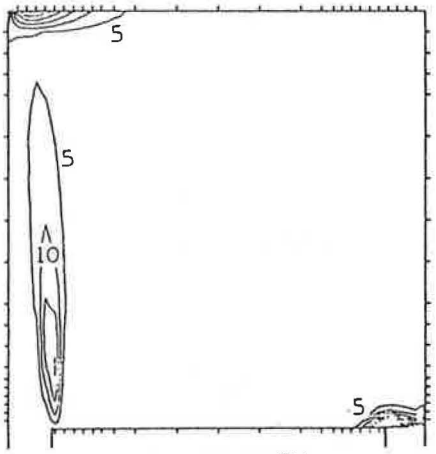

($\varepsilon \times 10^{-3}$)

ε Distribution

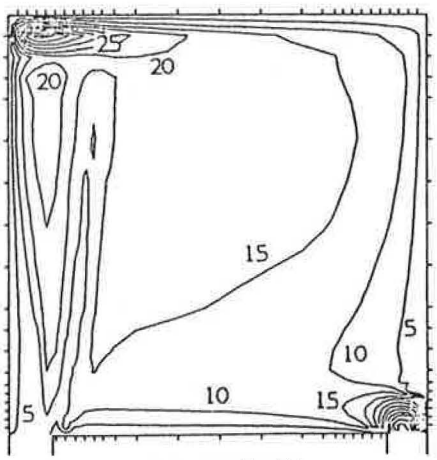

($\nu_t \times 10^{-3}$)

ν_t Distribution

(b) Schematic view of the sliced section of the gymnasium and positions of the supply outlets and the exhaust inlets

Figure 6 *Turbulence properties based on simulation with curvilinear coordinates*

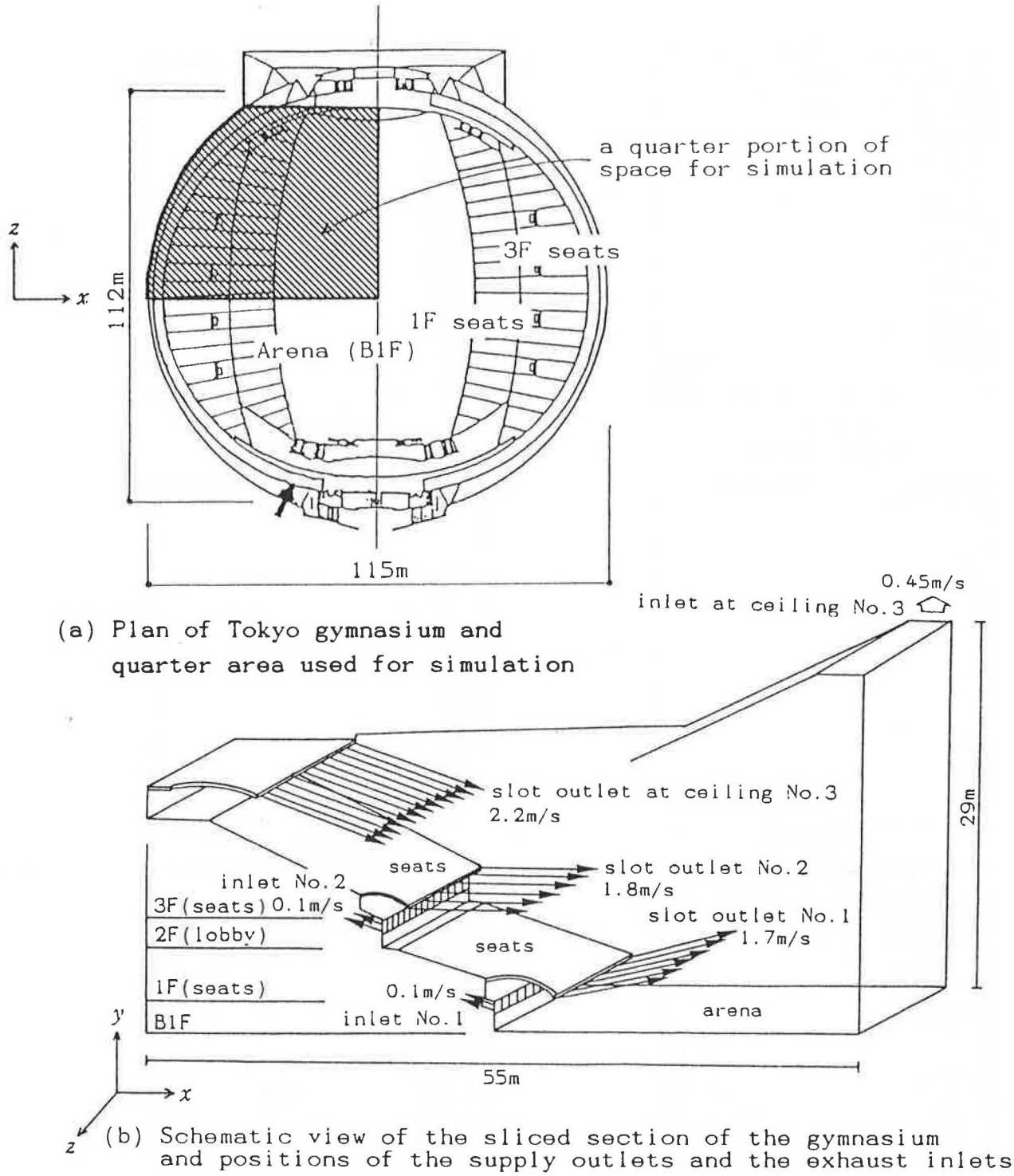

Figure 7 *Arrangement of supply and exhaust openings of Tokyo gymnasium*

accurately. Therefore, fine grid discretization is required at the area where steep gradients of dependent variables appear.

3-D Numerical Simulation of Air Distribution in a Gymnasium

The air distribution of the Tokyo Gymnasium, which is now under construction, is simulated (Kato et al. 1988). The k-ε model with no buoyancy effect is used. The gymnasium is divided into four parts by the two orthogonal center lines and one quarter is selected for simulation purposes (see Figures 7a and 7b) since this gymnasium space is symmetrical on both sides of either center line. We applied the three-dimensional analysis proposed in the appendices to this space. Since it has a very complicated configuration, the advantage of the present method over the preceding one based on Cartesian coordinates is confirmed.

Figure 7b is a schematic view of the section of the model near the center line. The model has two lines of

TABLE 6
Boundary Condition of Gymnasium Model

Supply outlet 1 : u^n=1.7, u^t=0.0, k=0.043, ℓ=0.08

Supply outlet 2 : u^n=1.8, u^t=0.0, k=0.049, ℓ=0.12

Supply outlet 3 : u^n=2.2, u^t=0.0, k=0.073, ℓ=0.12

Exhaust inlet 1 : u^n=0.1, u^t,k,ε: free-slip

Exhaust inlet 2 : u^n=0.1, u^t,k,ε: free-slip

Exhaust inlet 1 : u^n=0.54, u^t,k,ε: free-slip

Wall boundary (wall, seats, floor, ceiling) : m=1/7

Imaginary boundary

(two cut-out sides of the quarter portion of the space) : free-slip

Time increment (grid type 1) : Δt=0.1

Distance between physical wall and computational boundary : h=0.02

Relaxation factors (in the vicinity of the exhaust inlet) : ω^p=ω^u=0.5, ω^k=ω^ε=1.0

Relaxation factors (in the other region) : ω^p=ω^u=1.0, ω^k=ω^ε=1.0

* Representative values for normalization : U_o=1.0 m/sec, L_o=1.0 m/sec

supply slot outlets at the wall (No. 1, No. 2) and one line of the supply slot outlets at the ceiling (No. 3). There are two lines of exhaust inlets at the wall (No. 1, No. 2) and one line of exhaust inlets at the top of the ceiling (No. 3). Velocity values and turbulence properties are normalized by the characteristic velocity of 1.0 m/s and the characteristic length of 1.0 m, respectively. The time increment is also normalized by these characteristics. The boundary conditions are described in detail in Table 6.

Figure 8 Is a grid layout of an x-y plane at the center line (z = 0), which is generated by an algebraic grid generation method. The grid is not required to be orthogonal. We divide the width of a quarter of the z-direction into 10 segments. The pattern of the discretization of the x-y plane at each value of z is nearly equal to that at the center (z = 0).

The distribution of the velocity vectors at the center (z = 0) is shown in Figure 9. The air flows along the ceiling, although the direction of the outlet jet (No. 3) is aimed slightly downward. A similar distribution appears along the arena, where a jet is directed upward at outlet No. 1. These results seem reasonable on the basis of experimental results (Kato et al. 1988). Figure 10 is a flow visualization of this experiment.

Figure 11 shows a 3-D view of the trajection lines of small marker particles that compose streaklines. It must be noted that the trajection of the marker is calculated from the averaged flow field, not from the instantaneous turbulent flow field. The simulation results of the one-quarter model are then combined to form the flow field of the full space.

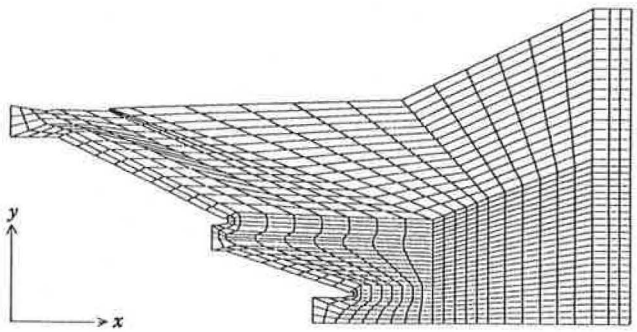

Figure 8 *Grid layout of x – y section (z = 0, center line)*

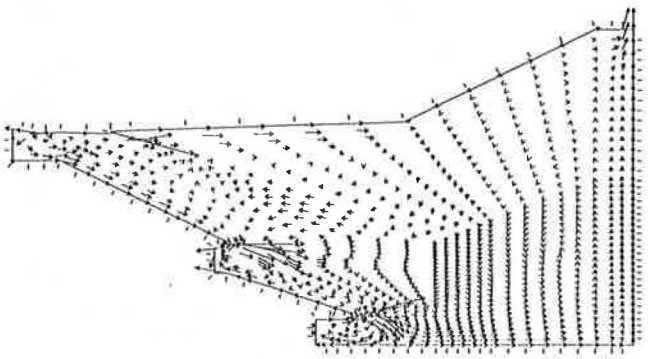

Figure 9 *Velocity vectors (u + v) (z = 0, center line)*

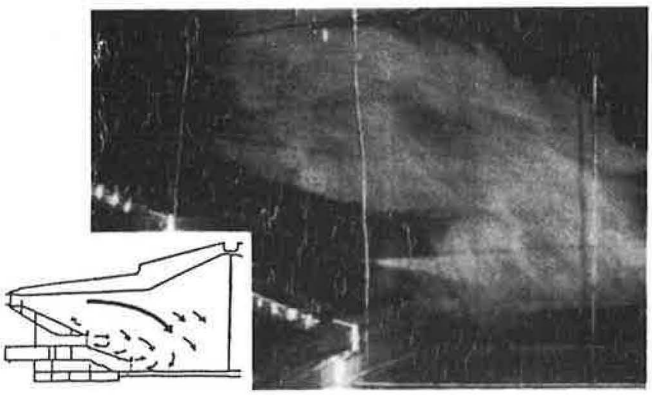

Figure 10 *Flow visualization*

The full space results combined by a computer graphics system satisfy the symmetrical condition with respect to the center lines. The emission of marker particles from three supply outlets begins at time 0. Figure 11a shows streaklines at time 95, (b) at time 300, and (c) at time 2500. Figure 11c shows the steady state of marker movement. Markers emitted from the left and right sides of the space are transported along the seats and the floor. They collide at the center of the arena at around time 300. Then markers are transported toward the ceiling, where the air is exhausted. Some three-dimensional standing vortices are observed in Figure 11c. One can comprehend precisely three-dimensional appearances of the flow field through a perspective view of 3-D simulation results by applying a computer graphics technique.

On the basis of the above results, the present method can be considered to be sufficiently practical and convenient for application to engineering problems.

Numerical Simulation of Air Distribution around a Two-dimensional Building Model

The air distribution around a two-dimensional square building model was simulated using the k-ϵ model. The numerical analysis of the external flow distribution around a building that has right-angled corners is very difficult because of the spatial singularity of these corners. The present simulation is a first step toward the three-dimensional simulation of external airflow distribution around arbitrarily shaped buildings.

The grid discretization of the entire computational domain around the building model is shown in Figure 12a. The enlarged one around the model is shown in Figure 12b. The grid lines of one curvilinear coordinate—constant ζ lines—radiate straight from the surface of the model and the grid lines of the other coordinate—constant lines—run across the former ones to form rectangular shapes that surround the model. All physical lengths are normalized by dividing by the length of one side of the square. The velocity and turbulence properties are normalized using the wind velocity of the height of the building model at the upwind inflow boundary. The time increment is also normalized by these characteristics. One side of the surface of the model is divided into 32 pieces. The sizes of the grid at the surface are 1/32 in wide and 1/20 in high in nondimensional length.

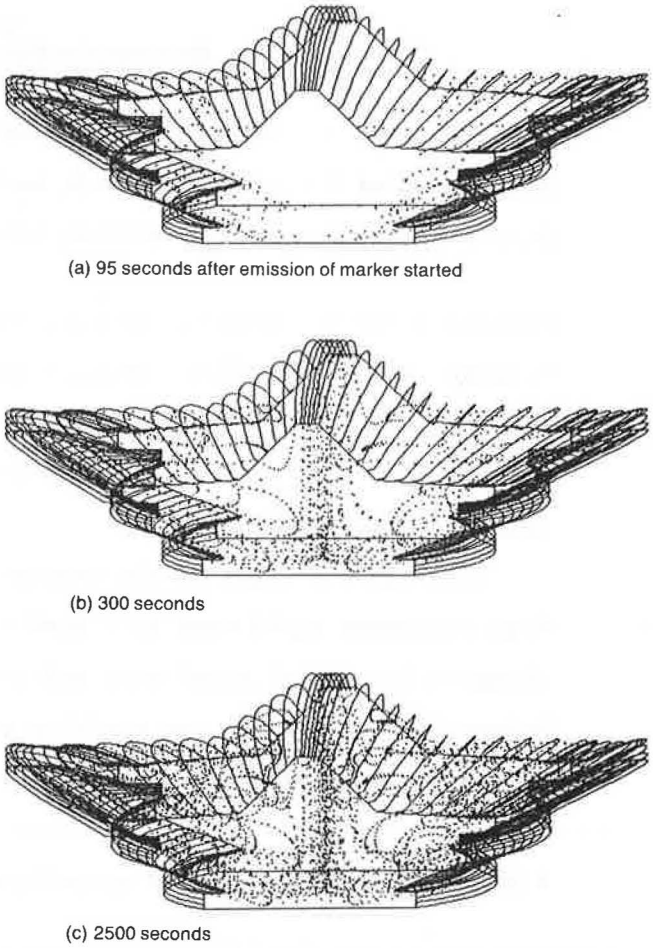

Figure 11 *Time-serial streaklines based on averaged flowfield (full space)*

At the boundary of the upwind inflow side (left side in Figure 13) and downwind outflow side of the region, velocity distributions are imposed by the power law. For velocity wall boundary conditions, the power law distributions are also assumed at the ground surface and the obstacle surface. The detail is illustrated in Table 7.

Figure 13 shows the simulation result of the stream lines of the entire region. The velocity vectors around the building model are shown in Figure 14. A backward flow is observed at the area in front of the model. A flow separation is generated at the front corner at the roof. A large wake is reproduced behind the model. Figure 15 shows the visualized flow field by the technique of a laser light sheet. The simulation result and the experimental one are similar.

Figure 16 shows the pressure distributions. A large pressure gradient is generated at the upwind corner of the obstacle. These distributions agree with expectations based on experience in wind engineering.

Figure 17 illustrates the distributions of the turbulence kinetic energy, k. Large values of k are observed at the upwind corner of the model. The values of k become smaller behind the model. Compared to the 3-D experimental results, the distribution pattern of k is close to the experimental one, but the values of k are larger than those of the 3-D experimental model.

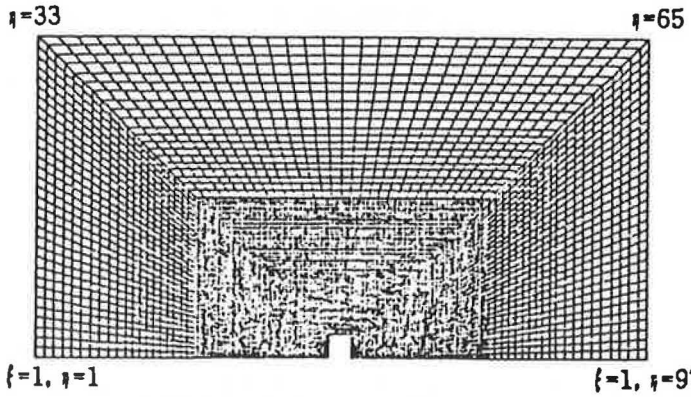

(a) Entire region for computation

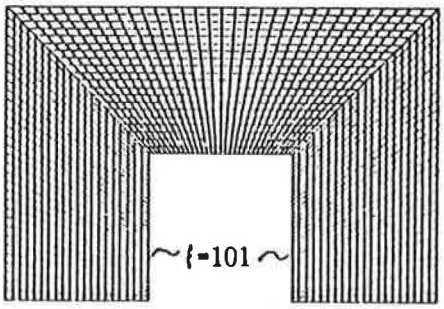

(b) Enlarged region around building model

Figure 12 *Grid discretization*

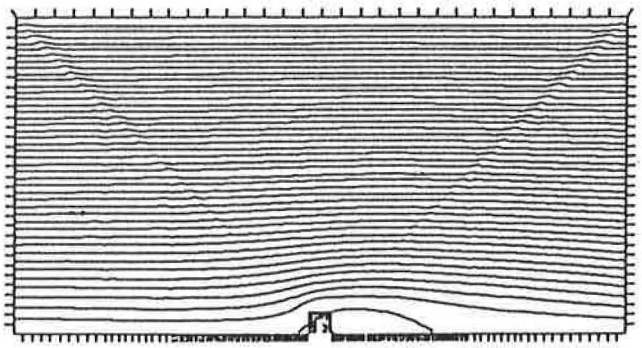

Figure 13 *Stream lines of entire region*

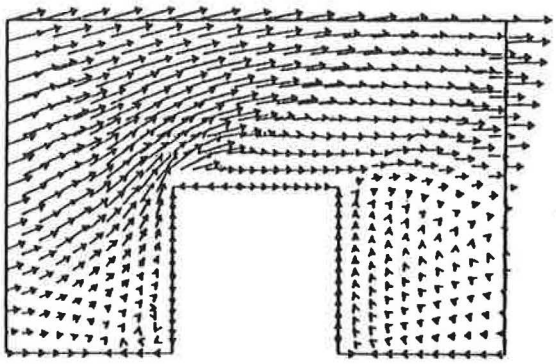

Figure 14 *Velocity vectors around building model*

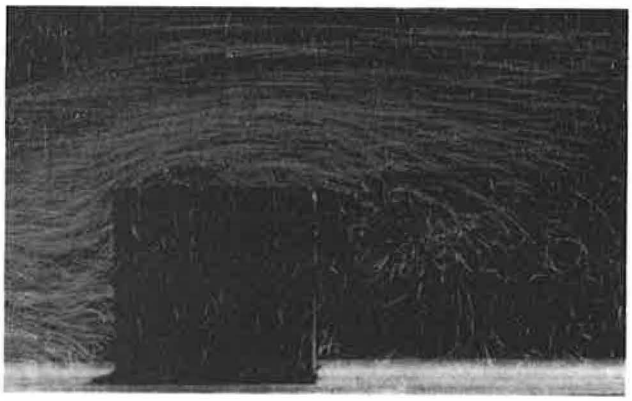

Figure 15 *Flow visualization by LLS*

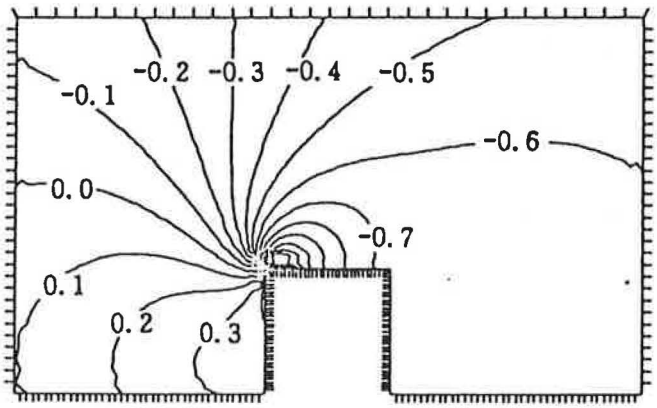

Figure 16 *Distribution of p around building model*

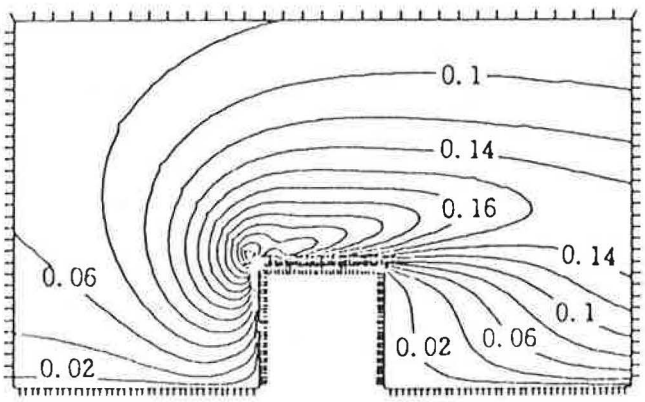

Figure 17 *Distribution of k*

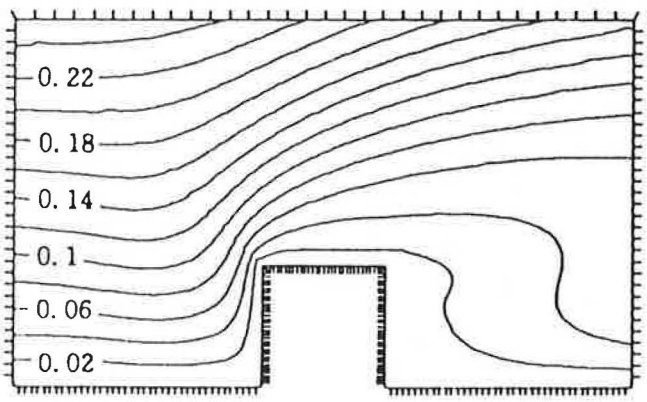

Figure 18 *Distribution of ν_t*

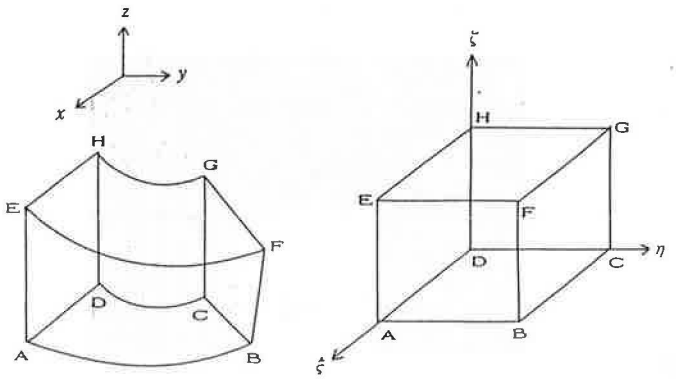

Figure 19 *Transformation from Cartesian coordinates to curvilinear coordinates*

Figure 18 shows the distribution of the kinematic viscosity, ν_t. The values of ν_t become small at the region near the model, which is the most important part of the entire region. This is a reasonable tendency. The value ν_t near the model depends on the value of h (distance between physical wall and computational boundary) because it is given by Equation 1.25 in Table 1 using values of the turbulence dissipation rate, ϵ, in Equation 2.22 in Table 2. Thus the value of h must be chosen carefully.

CONCLUSIONS

Three examples of numerical simulation that show good agreement with the experimental data are illustrated. First, the correctness of the present method is confirmed by comparing the present results of room airflow simula-

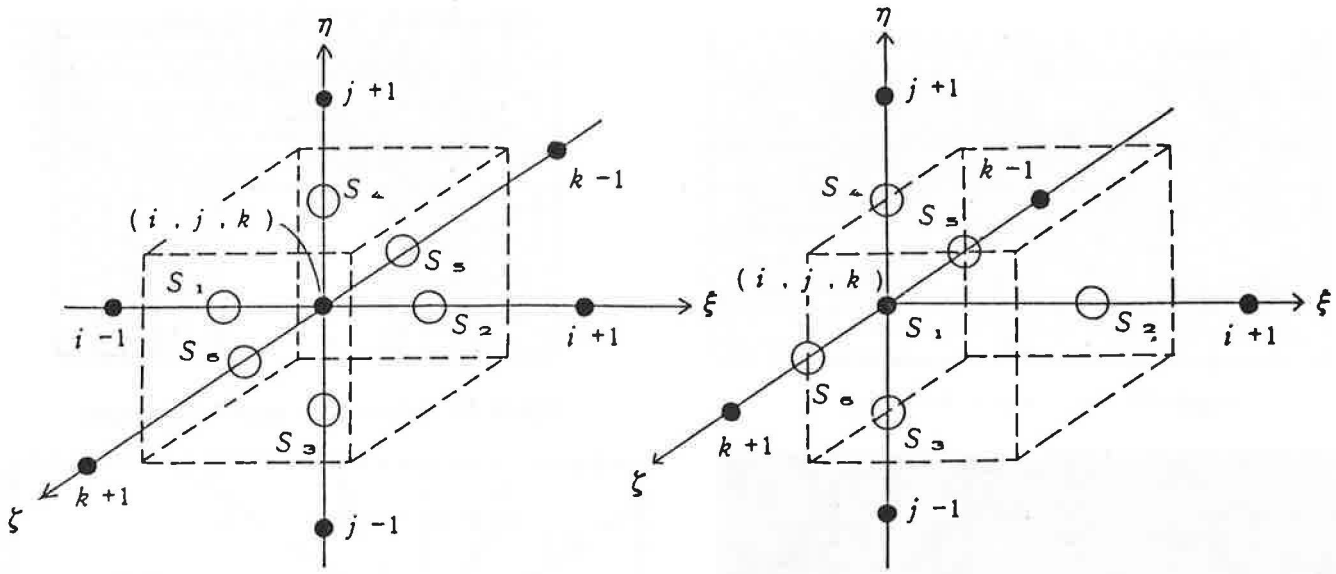

(a) Full control volume

(b) One-half control volume

Broken line rectangle expresses control volumes.
S_i means an area for surface integration.
(● = nodal point, ○ = midpoint of surface)

Figure 20 *Definition of control volume and surface for integration*

TABLE 7
Boundary Condition of Two-dimensional Building Model

Upwind inflow side : $u^n=(z)^{1/4}$, $u^t=0$, $k=0.025$, $\ell=1.18(z)^{1/4}$
Downwind outflow side : $u^n=(z)^{1/4}$, $u^t=0$, k, ϵ : free-slip
Ground and building surfaces : u^t : power-law (m=1/4), k : free-slip, ϵ : wall-law
Imaginary boundary (upper side of the region) : u^t, k, ϵ : free-slip
Front and rear corners at the roof : u=v=0
Time increment : $\Delta t=0.003$
Distance between physical wall and computational boundary : h=0.005
Relaxation factors : $\omega^p=\omega^u=0.9, \omega^k=\omega^\epsilon=1.0$

* Representative values for normalization

: L_o, height of building
U_o, wind velocity at the level of building height

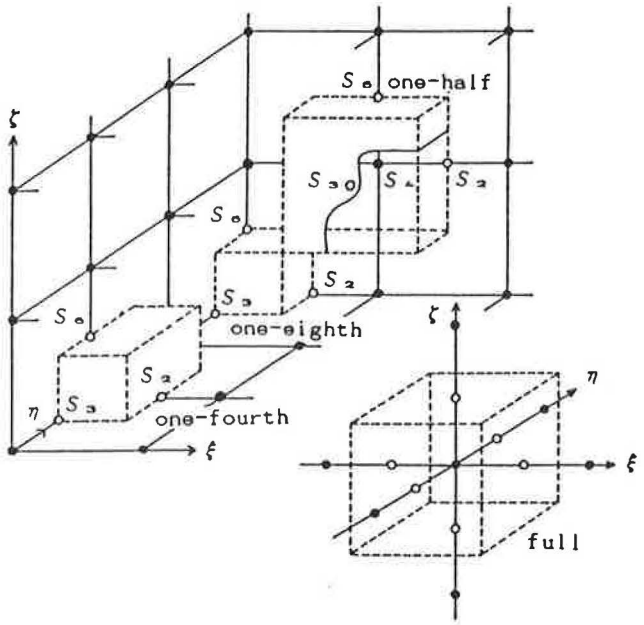

Figure 21 *Types of control volumes, full, one-half, one-fourth, and one-eighth (defined in relation to boundary)*

tion with results obtained from the existing numerical method, as well as with experimental results.

Second, the practicability of the present method is demonstrated by simulating the airflow in a gymnasium that has a complicated boundary configuration.

Finally, airflow distributions around a two-dimensional building model are presented. This example shows the possibility of three-dimensional simulations of external airflow distributions around arbitrarily shaped buildings.

These practical analyses confirm the present method as excellent for analyzing flow fields with complex-shaped boundaries.

In the appendices the authors show the method by which the k-ϵ model equations expressed by the Cartesian coordinates are transformed to those expressed by the generalized curvilinear system. Discrete equations using a regular grid system are deduced based on the control volume method. A new type of formulation for boundary conditions is also proposed. The relaxation method for the momentum equations using the contravariant vector and for the Poisson equation is expressed, as well as the relaxation equations of the transport equations of k and ϵ.

NOMENCLATURE

x, y, z	=	physical or Cartesian coordinates
$\xi, \eta, \zeta,$	=	computational coordinates or generalized curvilinear coordinates
u, v, w	=	x, y, z components of the velocity vector
U, V, W	=	components of the contravariant vector of velocity (cf. Equation C-2)
p	=	kinematic total mean pressure (usually defined as $[p/\rho + (2/3)k]$ where ρ is density)
k	=	turbulence kinetic energy
ϵ	=	turbulence dissipation rate
ν_t	=	eddy kinematic viscosity
ℓ	=	length scale of turbulence

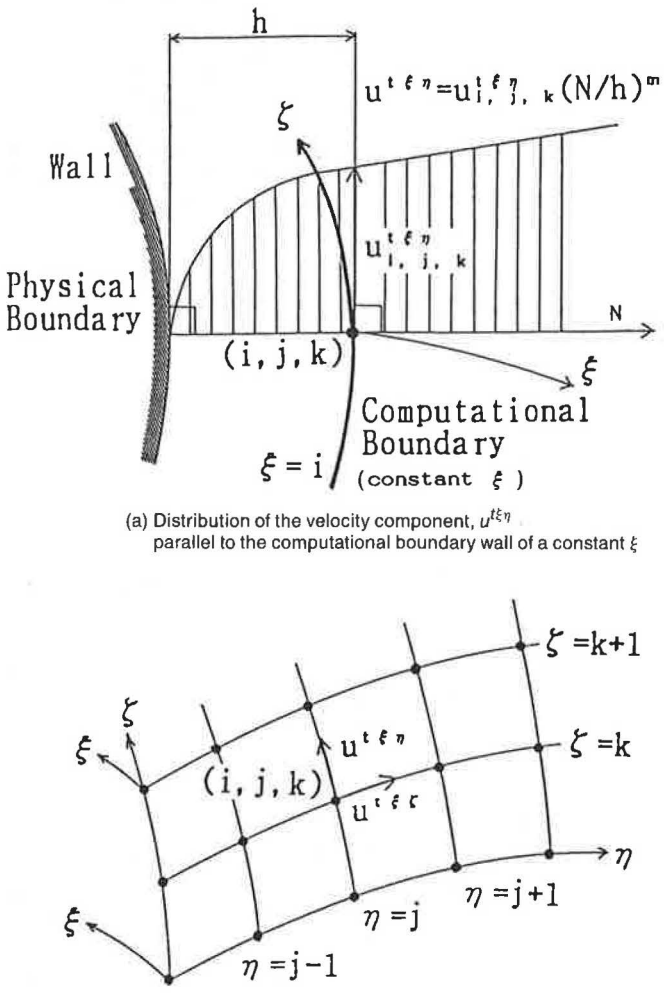

(a) Distribution of the velocity component, $u^{t\xi\eta}$ parallel to the computational boundary wall of a constant ξ

(b) Definition of the velocity components $u^{t\xi\eta}$ and $u^{t\xi\zeta}$ parallel to the boundary with a constant ξ

Figure 22 *Boundary condition of the velocity given by the power law*

$\square^{t\xi\eta}$	=	tangential velocity component parallel to the constant ξ surface in the direction of the ζ-curve (namely, tangential component parallel to a curve with constant $\xi$and constant η)
h	=	distance between computational and physical boundary surfaces

Subscripts and Superscripts

$\square_{i,j,k}$	=	discrete value at the nodal point (i, j, k) with respect to generalized curvilinear coordinates $\xi = i$, $\eta = j$, $\zeta = k$
$\square^n$	=	value at time step, n
${}^{\ell}\square$	=	value at iteration time, ℓ, of the relaxation calculation
$\square_t$	=	partial derivative with respect to the time, t
$\square_x, \square_y, \square_z$	=	partial derivatives with respect to the Cartesian coordinates, namely with respect to x, y, z, respectively
$\square_\xi, \square_\eta, \square_\zeta$	=	partial derivatives with respect to the generalized curvilinear coordinates, namely with respect to ξ, η, or ζ, respectively
$(\square, \square, \square)$	=	expression of a vector in the physical region, namely in the Cartesian coordinates

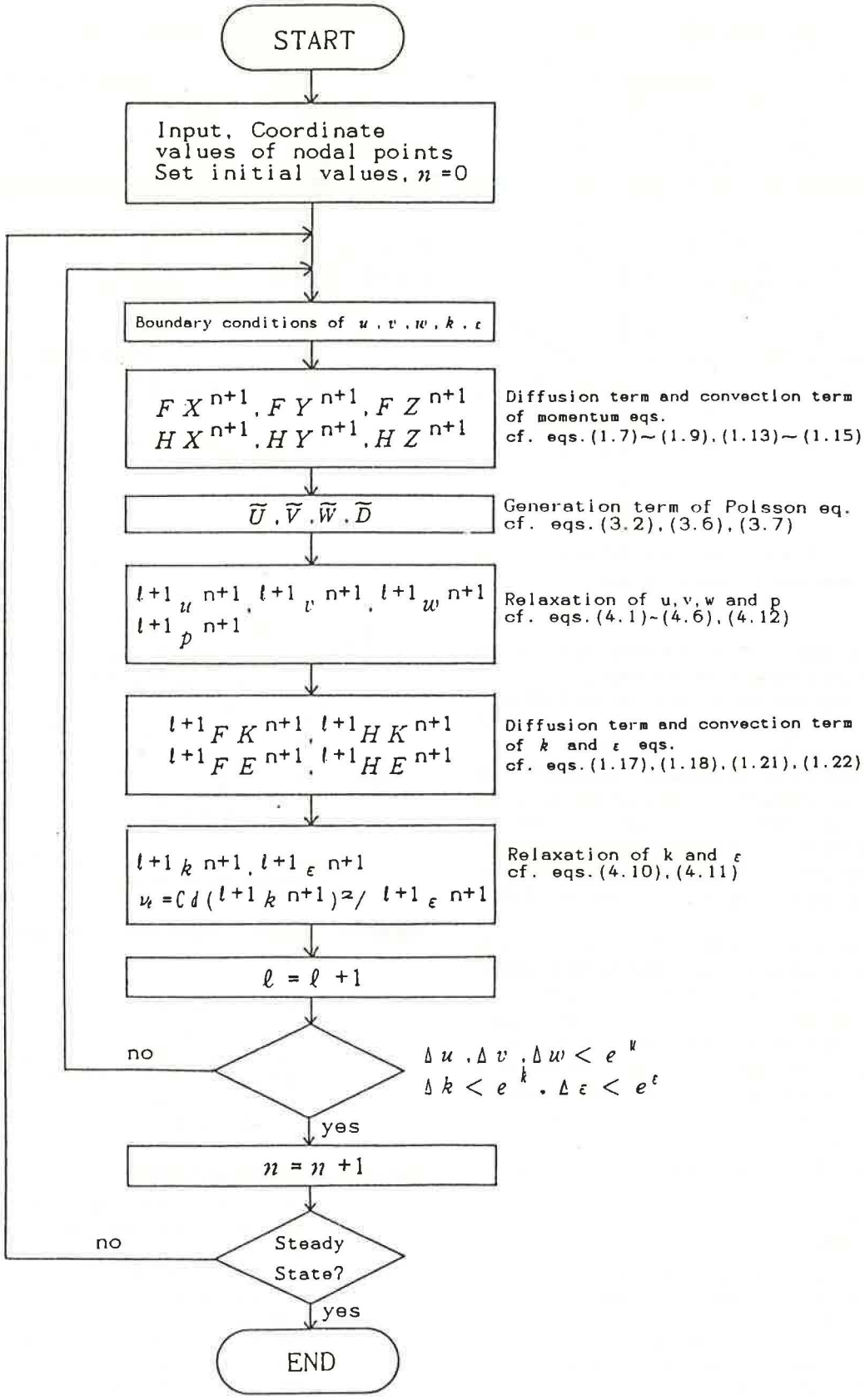

Figure 23 *Flow chart of time marching procedure*

REFERENCES

Harlow, F.H., and Welch J.E. 1965. "Numerical calculation of time-dependent viscous incompressible flow of fluid with free surface." *Phys. Fluids*, Vol. 8, pp. 2182-2189.

Kato, S., and Murakami, S. 1988. "New ventilation efficiency scales based on spatial distribution of contaminant concentration aided by numerical simulation." *ASHRAE Transactions*, Vol. 94, Part 2, pp. 309-330.

Kato, S.; Murakami, S.; Kong, C.N.; and Nakagawa, N. 1988. "Model experiment on indoor climate and space air distribution in a large-scale room." International Symposium on Scale Modeling, July 18-22, Tokyo.

Leonard, B.P. 1980. "The QUICK algorithm: a uniformly third-order finite difference method for highly convective flows." *Computer Methods in Fluids*, pp. 159-195. London: Pentech Press.

Murakami, S.; Kato, S.; and Suyama, Y. 1987. "Three-dimensional numerical simulation of turbulent airflow in a ventilated room by means of a two-equation model." *ASHRAE Transactions*, Vol. 93, Part 2, pp. 621-642.

Murakami, S.; Kato, S.; and Suyama, Y. 1988. "Numerical and experimental study on turbulent diffusion fields in conventional flow type clean room." *ASHRAE Transactions*, Vol. 94, Part 2, pp. 469-493.

Murakami, S.; Kato, S.; and Ishida, Y. 1988. "Numerical simulation of room air flow with generalized curvilinear coordinates 1-2." *Journal of Architecture, Planning and Environmental Engineering (Transactions of AIJ)*, No. 386 (April), No. 391 (September).

Nomura, T.; Murakami, S.; Kato, S.; and Sato, S. 1980. "Correspondence of the three-dimensional numerical analysis of turbulence flow." *Transactions of the Architectural Institute of Japan*, No. 298 (December).

Rizk, Y.M. 1985. "Use of a hyperbolic grid generation scheme in simulating supersonic viscous flow about three-dimensional winged configurations." International Symposium on Computational Fluid Dynamics-Tokyo, Vol. 2 (September).

Thompson, J.F.; Warsi, Z.U.A., and Mastin, C.W. 1985. *Numerical grid generation*. New York: Elsevier Science Publishing Co. Inc.

Yeung, P.K., and Kot, S.C. 1985. "Computation of turbulent flows past arbitrary two-dimensional surface-mounted obstructions." *Journal of Wind Engineering and Industrial Aerodynamics*, Vol. 18, pp. 177-190.

APPENDIX A
TRANSFORMATION RELATIONS

The authors define the generalized curvilinear coordinates or the computational coordinates (ξ, η, ζ) related to the Cartesian coordinates (x, y, z) by transformation equations, as shown in Equation A-1.

$$\xi=\xi(x,y,z),\quad \eta=\eta(x,y,z),\quad \zeta=\zeta(x,y,z) \tag{A-1}$$

A relation between the curvilinear coordinates and the Cartesian coordinates is illustrated in Figure 19. No orthogonality conditions are imposed on the curvilinear coordinates here.

Next the Jacobian is defined as

$$J=\begin{vmatrix} x_\xi & x_\eta & x_\zeta \\ y_\xi & y_\eta & y_\zeta \\ z_\xi & z_\eta & z_\zeta \end{vmatrix} = \begin{vmatrix} \xi_x & \xi_y & \xi_z \\ \eta_x & \eta_y & \eta_z \\ \zeta_x & \zeta_y & \zeta_z \end{vmatrix}^{-1} \tag{A-2}$$

The metric elements and metric coefficients are connected by the following relations:

$$\begin{aligned}
&\xi_x=(y_\eta z_\zeta - y_\zeta z_\eta)/J,\quad \xi_y=-(x_\eta z_\zeta - x_\zeta z_\eta)/J,\quad \xi_z \\
&\quad =(x_\eta y_\zeta - x_\zeta y_\eta)/J, \\
&\eta_x=-(y_\xi z_\zeta - y_\zeta z_\xi)/J,\quad \eta_y=(x_\xi z_\zeta - x_\zeta z_\xi)/J,\quad \eta_z \\
&\quad =-(x_\xi y_\zeta - x_\zeta y_\xi)/J \\
&\zeta_x=(y_\xi z_\eta - y_\eta z_\xi)/J,\quad \zeta_y=-(x_\xi z_\eta - x_\eta z_\xi)/J,\quad \zeta_z \\
&\quad =(x_\xi y_\eta - x_\eta y_\xi)/J
\end{aligned} \tag{A-3}$$

Metric coefficients defined by x_ξ, x_η, x_ζ, y_ξ, y_η, y_ζ, z_ξ, z_η, and z_ζ are calculated using a central difference with respect to the physical coordinates; an example is shown in Equation A-4.

$$(x_\xi)_{i,j,k}=(x_{i+1,j,k}-x_{i-1,j,k})/(2\Delta\xi) \tag{A-4}$$

The value of the space increments in the computational region $\Delta\xi$, $\Delta\eta$, and $\Delta\zeta$ is set as unity. Metric elements defined by ξ_x, ξ_y, ξ_z, η_x, η_y, η_z, ζ_x, ζ_y, and ζ_z can be calculated using the above relations (A-3).

APPENDIX B
TRANSFORMATION FORMULAS FOR DIFFERENTIALS AND INTEGRALS

Equations B-1, B-2, and B-3 show the general conservative expression based on the curvilinear coordinates for a partial derivative f_x, f_y, and f_z for function f, where f(x, y, z) is $f\{x(\xi, \eta, \zeta), y(\xi, \eta, \zeta), z(\xi, \eta, \zeta)\}$.

$$\begin{aligned}
f_x&=\xi_x f_\xi+\eta_x f_\eta+\zeta_x f_\zeta \\
&=\{(J\xi_x f)_\xi+(J\eta_x f)_\eta+(J\zeta_x f)_\zeta\}/J.
\end{aligned} \tag{B-1}$$

$$\begin{aligned}
f_y&=\xi_y f_\xi+\eta_y f_\eta+\zeta_y f_\zeta \\
&=\{(J\xi_y f)_\xi+(J\eta_y f)_\eta+(J\zeta_y f)_\zeta\}/J
\end{aligned} \tag{B-2}$$

$$\begin{aligned}
f_z&=\xi_z f_\xi+\eta_z f_\eta+\zeta_z f_\zeta \\
&=\{(J\xi_z f)_\xi+(J\eta_z f)_\eta+(J\zeta_z f)_\zeta\}/J
\end{aligned} \tag{B-3}$$

The integration form with respect to a control volume V in curvilinear coordinates is expressed as:

$$\begin{aligned}
&\int_V f(x,y,z)dV=\int_{x1}^{x2}\int_{y1}^{y2}\int_{x1}^{x2} f(x,y,z)dxdydz \\
&=\int_{\zeta1}^{\zeta2}\int_{\eta1}^{\eta2}\int_{\xi1}^{\xi2} f\{x(\xi,\eta,\zeta),y(\xi,\eta,\zeta) \\
&,z(\xi,\eta,\zeta)\}Jd\xi d\eta d\zeta
\end{aligned} \tag{B-4}$$

APPENDIX C
TRANSFORMATION OF GOVERNING EQUATIONS OF k-ϵ MODEL

The governing equations expressed with Cartesian coordinates and the transformed expressions based on the curvilinear coordinates are shown in Table 1. In this section, "transformation relations" implies that the equations are being transformed from Cartesian coordinates to curvilinear coordinates. We express the transformation of the momentum equations as shown in Equations 1.4 through 1.15 in Table 1, where HX, HY, and HZ are the convection terms; p_x, p_y, and p_z are pressure gradient terms;

and FX, FY, and FZ are diffusion terms of the momentum equations. The transformation relations of transport equations of the turbulence kinetic energy, k, and the turbulence dissipation rate, ϵ, are shown in Equations 1.16 through 1.22 in Table 1. HK and HE are convection terms. FK and FE are diffusion terms.

The continuity equation by the Cartesian coordinates and the conservative expression based on the curvilinear coordinates are shown in Table 1 as Equation 1.1. The continuity equation is transformed as below by referring to formulas B-1 through B-3.

$$u_x+v_y+w_z = [\{J(\xi_x u+\xi_y v+\xi_z w)\}_\xi + \{J(\eta_x u+\eta_y v+\eta_z w)\}_\eta + \{J(\zeta_x u+\zeta_y v+\zeta_z w)\}_\zeta]/J=0 \quad \text{(C-1)}$$

A new vector (U, V, W) defined by the following equation as the contravariant vector of the velocity vector (u, v, w) is introduced.

$$U=\xi_x u+\xi_y v+\xi_z w,\quad V=\eta_x u+\eta_y v+\eta_z w,\quad W=\zeta_x u+\zeta_y v+\zeta_z w \quad \text{(C-2)}$$

U is proportional to the velocity vector component normal to the constant ξ curved surface, V is proportional to the velocity vector component normal to the constant η curved surface, and W is proportional to the velocity vector component normal to the constant ζ curved surface.

The following equations are obtained by solving Equation C-2 simultaneously in reference to Equations A-2 and A-3.

$$u=x_\xi U+x_\eta V+x_\zeta W,\quad v=y_\xi U+y_\eta V+y_\zeta W,\quad w=z_\xi U+z_\eta V+z_\zeta W$$

$$FX=\{\nu_e(u_x-v_y-w_z)\}_x+\{\nu_e(u_y+v_x)\}_y+\{\nu_e(u_z+w_x)\}_z$$

$$=[\{J\nu_e(\xi_x u_x+\xi_y u_y+\xi_z u_z-\xi_x v_y-\xi_x w_z+\xi_y v_x+\xi_z w_x)\}_\xi \quad \text{(C-3)}$$

Next, the authors will explain the method by which the diffusion term of the momentum equation of the x-direction is transformed from Cartesian coordinates to curvilinear coordinates. As is shown in Equation 1.13 in Table 1, u_x in the diagonal component of the strain rate tensor is changed by the continuity equation. This is also performed for v_y of Equation 1.14 and w_z of Equation 1.15. Simple expressions are obtained by this substitution, as will be illustrated later. The following equations are derived by referring to formulas B-1, B-2, and B-3.

$$+\{J\nu_e(\eta_x u_x+\eta_y u_y+\eta_z u_z-\eta_x v_y-\eta_x w_z+\eta_y v_x+\eta_z w_x)\}_\eta$$

$$+\{J\nu_e(\zeta_x u_x+\zeta_y u_y+\zeta_z u_z-\zeta_x v_y-\zeta_x w_z$$

$$+\zeta_y v_x+\zeta_z w_x)\}_\zeta]/J \quad \text{(C-4)}$$

Then, by substituting $u_x = \xi_x u_\epsilon + \eta_x u_\eta + \zeta_x u_\zeta$ and likewise for the variables u_y, u_z, v_x, v_y, etc., into Equation C-4, the diffusion term is rearranged as below:

The transformation relations for the y-direction and z-direction diffusion terms are obtained in the same way. The pressure terms are changed simply by substituting p in Equations B-1, B-2, and B-3. The transformations of the transport equations of k and ϵ, using a similar technique, are performed more easily than those of the momentum equations.

Applying the above transformation procedures to the governing equations of the k-ϵ model, one can introduce the transformed expressions of the governing equations based on the curvilinear coordinates shown in Table 1, where the convection terms, the pressure gradient terms, and the diffusion terms are denoted conservatively. This conservative expression is very important since errors due to the numerical integration may be greatly reduced by this expression.

APPENDIX D
DISCRETIZATION

Discretization by the Control Volume Method

We use here the regular grid system in which all dependent variables are defined at the same nodal points in the discretized three-dimensional region, as shown in Figure 20. The discrete governing equations are obtained by integrating the governing equations with each control volume. Many shapes of the control volume appear to be related to the boundary, as shown in Figure 21.

We can express the convection terms, diffusion terms, and pressure gradient terms of the governing equations in the same form as Equation D-1 because these terms, which are called transport terms, have been denoted conservatively with respect to the curvilinear coordinates, as shown in Table 1.

$$F=(A_\xi+B_\eta+C_\zeta)/J \quad \text{(D-1)}$$

A budget of flux through surfaces of a finite control volume is estimated by integrating each term within the control volume. By integrating Equation D-1, the following discretized expression is obtained:

$$\int_v F dV=\int_{k-1/2}^{k+1/2}\int_{j-1/2}^{j+1/2}\int_{i-1/2}^{i+1/2} F J d\xi d\eta d\zeta$$

$$\doteq A(i+1/2,j,k)-A(i-1/2,j,k)$$

$$+B(i,j+1/2,k)-B(i,j-1/2,k)$$

$$+C(i,j,k+1/2)-C(i,j,k-1/2) \quad \text{(D-2)}$$

For the half-shaped control volume that coincides with the boundary at S_1, as shown in Figure 20b, the following discrete

$$FX=[J\nu_e\{(\xi_x^2+\xi_y^2+\xi_z^2)u_\xi+(\xi_x\eta_x+\xi_y\eta_y+\xi_z\eta_z)u_\eta+(\xi_x\zeta_x+\xi_y\zeta_y+\xi_z\zeta_z)u_\zeta$$
$$-(z_\zeta/J)v_\eta+(z_\eta/J)v_\zeta+(y_\zeta/J)w_\eta-(y_\eta/J)w_\zeta\}]_\xi/J$$
$$+[J\nu_e\{(\eta_x\xi_x+\eta_y\xi_y+\eta_z\xi_z)u_\xi+(\eta_x^2+\eta_y^2+\eta_z^2)u_\eta+(\eta_x\zeta_x+\eta_y\zeta_y+\eta_z\zeta_z)u_\zeta$$
$$+(z_\zeta/J)v_\xi-(z_\xi/J)v_\zeta-(y_\zeta/J)w_\xi+(y_\xi/J)w_\zeta\}]_\eta/J$$
$$+[J\nu_e\{(\zeta_x\xi_x+\zeta_y\xi_y+\zeta_z\xi_z)u_\xi+(\zeta_x\eta_x+\zeta_y\eta_y+\zeta_z\eta_z)u_\eta+(\zeta_x^2+\zeta_y^2+\zeta_z^2)u_\zeta$$
$$-(z_\eta/J)v_\xi+(z_\xi/J)v_\eta+(y_\eta/J)w_\xi-(y_\xi/J)w_\eta\}]_\zeta/J \quad \text{(C-5)}$$

equation is obtained by integrating Equation D-1 with respect to the one-half control volume:

$$\int_v F dV = \int_{k-1/2}^{k+1/2}\int_{j-1/2}^{j+1/2}\int_{i}^{i+1/2} F J d\xi d\eta d\zeta$$

$$\doteqdot A(i+1/2,j,k)-A(i,j,k)$$

$$+\{B(i,j+1/2,k)-B(i,j-1/2,k)\}/2$$

$$+\{C(i,j,k+1/2)-C(i,j,k-1/2)\}/2 \qquad \text{(D-3)}$$

The integration area is changed similarly for the one-fourth-shaped or one-eighth-shaped control volume, shown in Figure 21. An integration for a term that cannot be expressed as the form of the surface integration is represented by the value at the nodal point, namely a value at the center of the control volume. For example, the integration of the production term of the transport equation of k is expressed as follows:

$$\int_v \nu_t S dV = \int_{k-1/2}^{k+1/2}\int_{j-1/2}^{j+1/2}\int_{i-1/2}^{i+1/2} \nu_t S J d\xi d\eta d\zeta$$

$$= (J \nu_t S)_{i,j,k} \qquad \text{(D-4)}$$

After applying the above-approximated integration formulas (D-2 or D-3) to each governing equation, an algebraic equation of discrete dependent variables is obtained at each nodal point. These algebraic equations can be solved at all nodal points simultaneously using a relaxation method, which will be discussed in Appendix H.

QUICK Scheme

The QUICK scheme is applied to the convection term of momentum equations (Leonard 1980; Murakami et al. 1987). When expressing the convection term as a form of Equation D-1, the terms A(i−1/2, j, k) and A(i+1/2, j, k) in Equation D-2 mean the momentum flux through the surface with a constant ξ. The momentum flux is expressed as follows by the QUICK method:

$$A(i-1/2,j,k) = [\{(JU)_{i-1,j,k}+(JU)_{i,j,k}\}/2]$$

$$\{(u_{i-1,j,k}+u_{i,j,k})/2-CURVN/8\} \qquad \text{(D-5)}$$

where CURVN/8 indicates the upwind effect, namely,

if $U_{i-1/2,j,k} > 0$

$$CURVN = u_{i-2,j,k}-2u_{i-1,j,k}+u_{i,j,k} \qquad \text{(D-6)}$$

or else, $U_{i-1/2,j,k} < 0$

$$CURVN = u_{i-1,j,k}-2u_{i,j,k}+u_{i+1,j,k}. \qquad \text{(D-7)}$$

The QUICK scheme is applied to the convection terms of the transport equations of k and ϵ in the same way as was described above.

APPENDIX E
BOUNDARY CONDITIONS

Here, the wall boundary condition is stated primarily because the inflow or the outflow boundary condition can be dealt with easily. In a curvilinear coordinate system, the boundary surface is to be treated as a curved surface with a constant value of ξ, η, or ζ, regardless of the boundary's degree of complexity. This property of the computational boundary allows one to formulate the boundary conditions simply.

In the present method, the imaginary computational boundary is set just inside the physical region of the flow field. The computational boundary surface is parallel to the physical boundary surface and separated from it by the small distance, h. Thus, the narrow area between the physical boundary and the computational boundary is not treated directly by the computation. With this positioning of the boundary, velocity components at the computational boundary, as well as those within the inner flow region, may be calculated using the momentum equations. The physical boundary imposes its boundary conditions on the computational boundary, which is set just inside the physical surface, using the proper wall law or wall function. Consequently, simple expressions for the boundary conditions are obtained, as will be mentioned below.

Wall Boundary Condition of Velocity Components by Power Law Distribution

Here, the authors deal with the constant ξ boundary surface. It is assumed that the tangential velocity components parallel to the computational boundary surface, namely parallel to the physical surface with constant ξ, satisfy the power law in the η-direction and ζ-direction. Based on this assumption, partial derivatives for the velocity components at the wall, u_ξ, v_ξ, and w_ξ are derived. These derivations are required to solve the momentum equations at the wall boundary.

The tangential velocity components are defined as $u^{t\xi\eta}$, which has the direction of the ζ-curve, and $u^{t\xi\zeta}$, which has the direction of the η-curve in Figure 22. Both $u^{t\xi\eta}$ and $u^{t\xi\zeta}$ are components of the velocity parallel to the computational boundary surface with a constant ξ. These tangential velocity components are expressed using the tangential unit vector at the nodal point (i, j, k) on the computational boundary surface as follows:

$$u^{t\xi\eta} = (u,v,w)\cdot(x_\zeta, y_\zeta, z_\zeta)/(x_\zeta^2+y_\zeta^2+z_\zeta^2)^{1/2} \qquad \text{(E-1)}$$

$$u^{t\xi\zeta} = (u,v,w)\cdot(x_\eta, y_\eta, z_\eta)/(x_\eta^2+y_\eta^2+z_\eta^2)^{1/2} \qquad \text{(E-2)}$$

It is assumed that both $u^{t\xi\eta}$ and $u^{t\xi\zeta}$ obey the power law, as illustrated in Figure 22. N is defined as a normal distance measured from the physical surface. Then the power law is expressed as Equation E-3 and two normal derivatives of the tangential velocity components are derived from differentiating Equation E-3 at the nodal point (i, j, k) (Equations E-4 and E-5).

$$u^{t\xi\eta} = u^{t\xi\eta}{}_{i,j,k}(N/h)^m, \quad u^{t\xi\zeta} = u^{t\xi\zeta}{}_{i,j,k}(N/h)^m \qquad \text{(E-3)}$$

$$(\partial u^{t\xi\eta}/\partial N)_{i,j,k} = (m/h)u^{t\xi\eta}{}_{i,j,k} \qquad \text{(E-4)}$$

$$(\partial u^{t\xi\zeta}/\partial N)_{i,j,k} = (m/h)u^{t\xi\zeta}{}_{i,j,k} \qquad \text{(E-5)}$$

The continuity equation is added with non-conservative form as follows:

$$u_x+v_y+w_z = \xi_x u_\xi+\xi_y v_\xi+\xi_z w_\xi+\eta_x u_\eta+\eta_y v_\eta+\eta_z w_\eta$$
$$+\zeta_x u_\zeta+\zeta_y v_\zeta+\zeta_z w_\zeta = 0 \qquad \text{(E-6)}$$

Using the above equations (E-1, E-2, E-4, E-5, and E-6), through some complicated algebraic procedures one can get partial derivatives u_ξ, v_ξ, and w_ξ for velocity components with respect to curvilinear coordinates, as shown in Table 2.

Wall Boundary Condition of Turbulence Kinetic Energy k by Free-Slip Condition

The gradient of k normal to the surface of the boundary vanishes under the free-slip condition. The free-slip condition of k can be expressed easily, as shown in Equations 2.7, 2.14, and 2.21 in Table 2.

Wall Boundary Condition of Turbulence Dissipation Rate by Wall Law

The authors have located a nodal point (i, j, k) at the computational boundary normal to the wall and a small normal distance, h, from the physical boundary, as shown in Figure 22a. The value of the turbulence dissipation rate at this point can be calculated easily using Equation 2.22 in Table 2.

APPENDIX F
TIME INTEGRATION METHOD

The momentum equations are approximated by means of a fully implicit scheme for the time integration as follows:

$$u^{n+1}=u^{n}+\Delta t\{-p_x{}^{n+1}-HX^{n+1}+FX^{n+1}\} \quad \text{(F-1)}$$

$$v^{n+1}=v^{n}+\Delta t\{-p_y{}^{n+1}-HY^{n+1}+FY^{n+1}\} \quad \text{(F-2)}$$

$$w^{n+1}=w^{n}+\Delta t\{-p_z{}^{n+1}-HZ^{n+1}+FZ^{n+1}\}, \quad \text{(F-3)}$$

where Δt is the time increment. The computational stability through the time marching procedure improves by applying the fully implicit scheme. Consequently a comparably larger time increment, Δt, can be used.

The continuity equation at the time step (n + 1) is expressed as follows:

$$u_x{}^{n+1}+v_y{}^{n+1}+w_z{}^{n+1}=0 \quad \text{(F-4)}$$

The following Poisson equation is obtained after substituting Equations F-1, F-2, and F-3 into Equation F-4:

$$p_{xx}{}^{n+1}+p_{yy}{}^{n+1}+p_{zz}{}^{n+1}$$
$$=(u^{n}{}_x+v^{n}{}_y+w^{n}{}_z)/\Delta t-(HX_x{}^{n+1}+HY_y{}^{n+1}+HZ_z{}^{n+1})$$
$$+(FX_x{}^{n+1}+FY_y{}^{n+1}+FZ_z{}^{n+1}) \quad \text{(F-5)}$$

Here, we must solve Equation F-5 and the momentum equations (Equations F-1, F-2, and F-3) simultaneously because HX^{n+1}, HY^{n+1}, HZ^{n+1}, FX^{n+1}, FY^{n+1}, and FZ^{n+1} are unknowns. We also apply the fully implicit scheme to the transport equations of k and ϵ.

APPENDIX G
SOLVING POISSON EQUATION OF PRESSURE

Formulation of Equation and Treatment at Boundary

After transforming Equation F-5 into curvilinear coordinates, it is integrated with respect to a control volume. Then, the transformed Poisson equation is obtained as shown in Equations 3.1 through 3.7 in Table 3. The superscript ($^{n+1}$) of the pressure is neglected. $\bar{D}$ is the generation term of the Poisson equation. It comes from the control volume integration of the right-hand side of Equation F-5. L_i is the coefficient that distinguishes whether or not the surface of the control volume coincides with the boundary, as shown in Equation 3.5 in Table 3. $\bar{U}$, $\bar{V}$, and $\bar{W}$ are defined in Equations 3.6 and 3.7 in Table 3.

A velocity component normal to the boundary surface is set at zero on the wall or it is given before as a fixed value at the supply outlet or the exhaust inlet. Using the above condition of the normal velocity component, the terms of the normal pressure gradient can be eliminated from the integrated Poisson equation by substituting the momentum equations in the Poisson equation. L_i in Equation 3.1 comes from this process of eliminating p.

APPENDIX H
RELAXATION METHOD

The momentum equations and the transport equations of k and ϵ must be solved simultaneously by the relaxation method because they are formulated with the fully implicit scheme. The relaxation method-which is used for the turbulence kinetic energy, k, turbulence dissipation rate, ϵ, and the pressure is an ordinary one, as is shown in Table 4. However, for the velocity components, a new method is proposed which imposes the Dirichlet-type boundary condition on the momentum equations automatically through the procedure of iterative calculations using contravariant vector components. The relaxation procedure of this method is shown in detail in Table 4.

In the present method a fully implicit scheme is used, so velocity components, pressure, turbulence kinetic energy, and turbulence dissipation rate are relaxed simultaneously in the same iteration loop. A calculation procedure of the present method is illustrated in Figure 23.